

BEYOND SEQUENCE: IMPACT OF GEOMETRIC CONTEXT FOR RNA PROPERTY PREDICTION

Anonymous authors

Paper under double-blind review

ABSTRACT

Accurate prediction of RNA properties, such as stability and interactions, is crucial for advancing our understanding of biological processes and developing RNA-based therapeutics. RNA structures can be represented as 1D sequences, 2D topological graphs, or 3D all-atom models, each offering different insights into its function. Existing works predominantly focus on 1D sequence-based models, which overlook the geometric context provided by 2D and 3D geometries. This study presents the first systematic evaluation of incorporating explicit 2D and 3D geometric information into RNA property prediction, considering not only performance but also real-world challenges such as limited data availability, partial labeling, sequencing noise, and computational efficiency. To this end, we introduce a newly curated set of RNA datasets with enhanced 2D and 3D structural annotations, providing a resource for model evaluation on RNA data. Our findings reveal that models with explicit geometry encoding generally outperform sequence-based models, with an average prediction RMSE reduction of around 12% across all various RNA tasks and excelling in low-data and partial labeling regimes, underscoring the value of explicitly incorporating geometric context. On the other hand, geometry-unaware sequence-based models are more robust under sequencing noise but often require around $2 - 5\times$ training data to match the performance of geometry-aware models. Our study offers further insights into the trade-offs between different RNA representations in practical applications and addresses a significant gap in evaluating deep learning models for RNA tasks. All datasets and code will be released upon acceptance.

1 INTRODUCTION

RNA plays a central role in the machinery of life, serving as a crucial intermediary between nucleotide and amino acid worlds (Sahin et al., 2014). Beyond its messenger role, RNA is involved in diverse biological processes, including gene regulation, catalytic activity, and structural support within ribosomes (Sharp, 2009; Strobel et al., 2016). This versatility makes RNA a key target for fundamental biological research and therapeutic interventions. As our understanding of RNA complexity grows, so does the need for advanced computational tools for its analysis.

Modeling RNA is challenging due to its intricate secondary and tertiary structures, dynamic conformational changes, and interactions with cellular components (Han et al., 2015). Furthermore, RNA analysis is hindered by the practical challenges of RNA data acquisition which include sequencing errors (Ozsolak & Milos, 2011), batch effects (Tran et al., 2020), incomplete sequencing (Alfonzo et al., 2021), partial labeling (Wayment-Steele et al., 2022b), and high costs of obtaining large labeled datasets (Byron et al., 2016). Moreover, RNA molecule can be represented in different ways: as a 1D nucleotide sequence, a 2D graph of base pairings, or a 3D atomic structure. Each representation highlights different aspects of RNA, presenting both opportunities and challenges for model design and selection (Fig. 1).

In this work, we systematically study the performance of various machine learning models for RNA property prediction, extending beyond traditional sequence-based approaches (He et al., 2021; Soylu & Sefer, 2023; Franke et al., 2022) to include methods that process RNA with its 2D or 3D geometry. While 2D and 3D RNA representations offer potentially richer information, they also present unique challenges. In the absence of high-quality experimental data, accessing 2D or 3D RNA structures re-

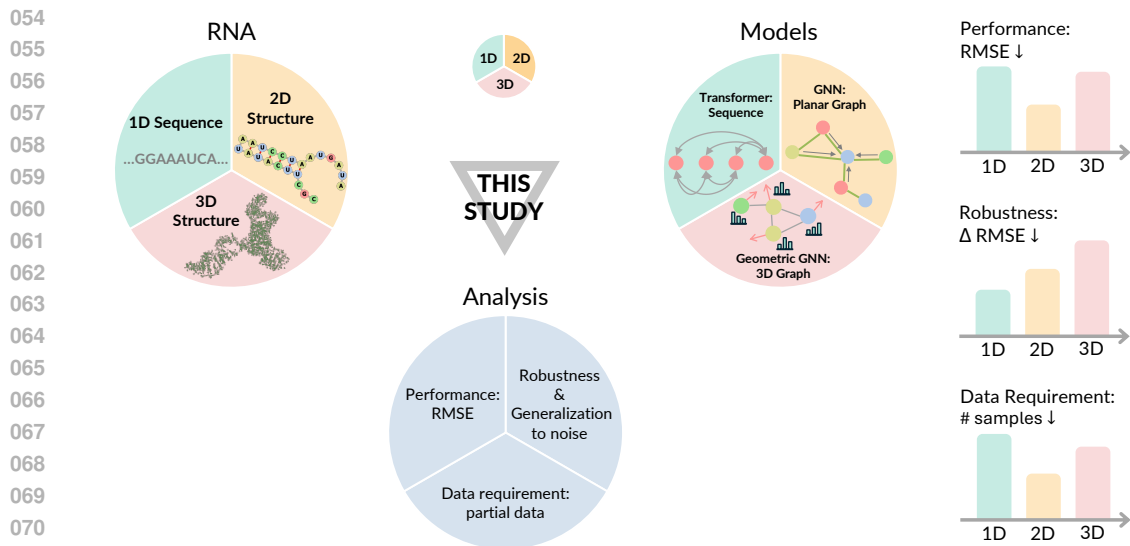


Figure 1: **Overview of the study.** (a) Left panel: RNA sequences represented in 1D, 2D, and 3D structures, processed by 1D sequence, 2D GNN, and 3D GNN models. Our analysis includes prediction error, robustness and generalization to sequencing noise, and performance under limited training data and partial labelings. (b) Right panel: Comparative performance of 1D, 2D, and 3D methods across experimental conditions. Histograms show RMSE performance, relative RMSE changes with increasing noise, and data requirements for optimal performance. Lower values indicate better performance in all metrics.

quires running structure prediction algorithms prone to noise and mistakes, especially in the presence of sequencing errors (Schneider et al., 2023; Wang et al., 2023). A few mutations in the nucleotide sequence owing to sequencing mistakes can hugely alter the 2D and 3D structure (Fig. 4), potentially undermining the benefit of using additional geometric context. Furthermore, real-world RNA datasets often suffer from partial labeling (Wayment-Steele et al., 2022b) and scarcity of training samples (Wint et al., 2022), which may affect geometry-aware methods differently than sequence-based approaches. These challenges raise a fundamental question: to what extent does explicit 2D and 3D geometry contribute to RNA property prediction, and under what circumstances might it offer advantages over geometry-free sequence models?

In this study, we seek to answer this question by making the following contributions:

- We introduce a diverse collection of RNA datasets, including newly annotated 2D and 3D structures, covering various prediction tasks at nucleotide and sequence levels across multiple species.
- We provide a unified testing environment to evaluate different types of machine learning models for RNA property prediction, including sequence models for 1D, graph neural networks for 2D, and equivariant geometric networks for 3D RNA representations.
- We conduct a comprehensive analysis of how different models perform under various conditions, such as limited data and labels, different types of sequencing errors, and out-of-distribution scenarios. We highlight the trade-offs and contexts in which each modeling approach is most effective, guiding researchers in selecting suitable models for specific RNA analysis challenges.
- We also introduce novel modifications to existing 3D geometric models based on biological prior, specifically optimizing them for handling large-scale point cloud RNA data, thus improving the efficiency and performance of 3D models significantly.

Our study reveals several key insights: **(i)** 2D models generally outperform 1D models, with spectral GNNs reducing prediction error by about 12% on average across all datasets, highlighting the importance of explicitly considering RNA structural information; **(ii)** 3D equivariant GNNs outperform 1D and some 2D methods in noise-free scenario but are sensitive to noise, exhibiting up to a 56% decrease in prediction quality under high sequencing error rates; **(iii)** geometry-free sequence models remain the most robust to sequencing noise, showing only a 14-27% increase in prediction

error compared to noise-free conditions, however they require around $2 - 5\times$ more training data to match the performance of geometry-aware models.

2 DATASETS AND MODELS

Here, we discuss datasets selected for our study with RNA-level prediction labels. These datasets are selected to vary from small to large-scale and to encompass both nucleotide-level tasks and sequence-level tasks. We perform an extensive evaluation across these datasets, leveraging three different model families (1D, 2D, 3D) spanning 9 representative models in total.

2.1 DATASETS

The datasets vary in size based on the number of sequences and sequence lengths: the small dataset Tc-Riboswitches (Groher et al., 2018), the medium datasets Open Vaccine COVID-19 (Wayment-Steele et al., 2022b) and Ribonanza-2k (He et al., 2024), and the large dataset Fungal (Wint et al., 2022). All datasets provide regression labels. Detailed statistics for these datasets are provided in Appendix F.1.

1. **Tc-Riboswitches:** 355 mRNA sequences (67-73 nucleotides) with sequence-level labels for tetracycline-dependent riboswitch switching behavior, important for optimizing gene regulation in synthetic biology and gene therapy.
2. **Open Vaccine COVID-19:** 4,082 RNA sequences (each of 107 nucleotides) with nucleotide-level degradation rate labels, crucial for predicting RNA stability in mRNA vaccine development.
3. **Ribonanza-2k:** 2,260 RNA sequences (each of 120 nucleotides) with nucleotide-level experimental reactivity labels, supporting RNA structure modeling and RNA-based drug design.
4. **Fungal:** 7,056 coding and tRNA sequences (150-3,000 nucleotides) from 450 fungal species, used for sequence-level protein expression prediction.

2.2 DATA PREPROCESSING AND CURATION

For the OpenVaccine COVID-19 dataset, we filter out sequences with a signal-to-noise ratio (SNR) below 1, as recommended by the dataset authors (Wayment-Steele et al., 2022b), to ensure that only sequences with a significant signal relative to background noise are included, thereby enhancing the reliability of modeling. For the other datasets, we use the original sequences since no SNR annotations are available.

Since all the RNA datasets come with sequences only, we employ EternaFold (Wayment-Steele et al., 2022a) and RhoFold (Shen et al., 2022) to infer 2D and 3D molecular structures respectively. We selected EternaFold and RhoFold due to their state-of-the-art performances acknowledged in recent works (Wayment-Steele et al., 2020; 2022b; He et al., 2024) Additionally, RhoFold typically runs in seconds to a minute per sequence, unlike other 3D structure prediction tools which usually take hours, and hence not suitable for large datasets.

For 1D modeling, we use the original RNA sequences without structural augmentation which equates to processing a plain string of nucleotides. The 2D datasets represent each RNA sequence as a graph with nodes for nucleotides and edges for bonds between nucleotides. The node features are six-dimensional, incorporating one-hot nucleotide identity ('A', 'C', 'G', 'U') alongside the sum and mean base-pairing probabilities (BPP), which are available from 2D structure prediction tools. In 3D, each RNA molecule is represented as a graph, with nodes corresponding to individual atoms. Node features represent one-hot atom identity.

2.3 MODELS

We select well-established model architectures recognized for their state-of-the-art performance for molecular property prediction tasks in various domains. **1D Model:** Transformer1D (Honda et al., 2019; He et al., 2021); **RNA-FM** (Chen et al., 2022), **SpliceBERT** (Chen et al., 2023) **2D Models:** GCN (Kipf & Welling, 2017; Wieder et al., 2020), GAT (Veličković et al., 2018; Ye et al., 2022), ChebNet (Defferrard et al., 2016; Knyazev et al., 2018), Transformer1D2D (He et al., 2023),

Graph Transformer (Shi et al., 2020; Li et al., 2022), and GraphGPS (Rampášek et al., 2022; Zhu et al., 2023); **3D Models:** SchNet (Schütt et al., 2017; Han et al., 2022), EGNN (Satorras et al., 2021), FAENet (Duval et al., 2023), DimeNet (Gasteiger et al., 2020), GVP (Jing et al., 2020), and FastEGNN (Zhang et al.). Detailed descriptions of all the models can be found in Appendix Sec. B.

Training and evaluation All models were trained on a NVIDIA A100 GPU. To ensure hyperparameter parity for each baseline, hyperparameters were optimized using Optuna (Akiba et al., 2019), restricting the search to models with fewer than 10 million parameters that fit within the GPU memory constraint of 80GB. All model hyperparameters, training, and evaluation details are reported in Appendix H. We ran all models for 5 random data splits (train:val:test split of 70:15:15) and we report average performance with a standard deviation across splits. The mean column-wise root mean squared error (MCRMSE), introduced in Wayment-Steele et al. (2020), is used as the evaluation metric. It is defined as $MCRMSE(f, D) = \sqrt{\frac{1}{n} \sum_{i=1}^n (\hat{y}_i - y_i)^2}$, where f represents a model, D is the dataset, and \hat{y}_i and y_i are the predicted and true values for data point i .

3 TASK DEFINITIONS

Here, we introduce the downstream tasks for evaluating models for RNA property prediction. Each task is designed to quantify specific behaviors under various real-world experimental conditions.

Task 1: Impact of structural information on prediction performance This task aims to evaluate how incorporating RNA structural information affects prediction quality. We compare the performance of models using 1D (sequence-only), 2D, and 3D RNA representations to determine if and to what extent geometric data improves property prediction.

Task 2: Model efficiency in limited training data settings Acquiring high-quality comprehensive RNA datasets is often challenging and resource-intensive thus limiting the amount of labeled data for training (Teufel & Sobetzko, 2022; Byron et al., 2016). This task aims to investigate how model performance depends on the amount of training data used, evaluating the sample efficiency of each family of models. In other words, given a dataset $D = \{X, Y\}$, let $D_\alpha = \{X_\alpha, Y_\alpha\}$ be a subset where the training set is reduced to a fraction α . We train models on different sets of D_α datasets with decreasing α .

Task 3: Performance with partial sequence labeling Due to the high cost of measuring properties for every nucleotide in RNA sequence, real-world datasets often contain partial annotations (Wayment-Steele et al., 2022b) where labels are only available for the first small part of the sequence. This task is relevant for nucleotide-level datasets and it aims to investigate how well a model can generalize to a whole RNA sequence when labels are only available for a portion of it.

Task 4: Robustness to sequencing noise Acquiring RNA data requires sequencing. In practice sequencing procedure may introduce sequencing errors (random mutations of nucleotides) that vary depending on the sequencing technology and platform (Ozsolak & Milos, 2011; Fox et al., 2014). These errors affect the raw sequence data, and propagate to structural noise in 2D and 3D. The goal of this task is to assess how well models can maintain reliable performance when trained and tested under the same distribution of realistic levels of sequencing noise observed in practice, ensuring robustness across a consistent noise environment. This reflects real-world cases where a specific sequencing method produces noisy data, but the noise characteristics are stable across training and deployment.

Task 5: Generalization to Out-of-Distribution (OOD) data This task focuses on a different practical challenge: models trained on high-quality RNA sequences are often deployed in conditions where the data exhibits different noise characteristics due to batch effect (Tran et al., 2020) or the use of different sequencing platforms (Tom et al., 2017). Here, the objective is to evaluate how well models generalize to OOD datasets with different levels of sequencing noise, assessing the extent of performance degradation as noise levels increase. This task simulates the scenario where a model encounters noisier data than it was trained on, highlighting its ability to adapt to unexpected experimental conditions.

Table 1: **Comparison of 1D, 2D, and 3D models across datasets.** **Bold** indicates the best, underline the second-best. ‘OOM’ means out-of-memory. ChebNet excels by capturing global graph information. Overall, 2D models outperform 1D models, highlighting the value of structural information. Although 3D models face challenges with scalability and noisy predictions, our nucleotide pooling strategy, based on biological prior, enhances their performance on shorter sequences, allowing 3D encoding to occasionally surpass 1D models. See Sec. 4.1 for details on nucleotide pooling strategy.

Model	COVID	Ribonanza	Tc-Ribo	Fungal
<i>1D model</i>				
Transformer1D	0.361±0.017	0.705±0.015	0.705±0.079	1.417±0.005
RNA-FM	<u>0.591±0.081</u>	0.99±0.144	<u>0.693±0.001</u>	<u>1.420±0.028</u>
SpliceBERT	<u>0.588±0.077</u>	<u>1.022±0.144</u>	<u>0.708±0.003</u>	<u>1.435±0.059</u>
<i>2D model</i>				
Transformer1D2D	0.305±0.012	0.514±0.004	0.633±0.001	OOM
GCN	0.359±0.009	0.595±0.006	0.701±0.004	1.192±0.077
GAT	0.315±0.006	0.534±0.006	0.685±0.024	1.112±0.035
ChebNet	0.279±0.007	0.468±0.002	0.621±0.022	0.973±0.003
Graph Transformer	0.318±0.008	0.515±0.001	0.710±0.041	1.317±0.002
GraphGPS	0.332±0.013	0.523±0.003	0.715±0.012	<u>1.025±0.081</u>
<i>3D model (w/o pooling)</i>				
EGNN (w/o pooling)	0.480±0.025	0.808±0.023	0.725±0.002	OOM
SchNet (w/o pooling)	0.499±0.003	0.843±0.004	0.696±0.008	OOM
FAENet (w/o pooling)	<u>0.486±0.010</u>	<u>0.834±0.003</u>	<u>0.703±0.011</u>	OOM
DimeNet (w/o pooling)	<u>0.497±0.012</u>	<u>0.855±0.006</u>	<u>0.712±0.004</u>	OOM
GVP (w/o pooling)	<u>0.467±0.010</u>	<u>0.797±0.012</u>	<u>0.744±0.004</u>	OOM
FastEGNN (w/o pooling)	<u>0.477±0.005</u>	<u>0.816±0.014</u>	<u>0.753±0.001</u>	OOM
<i>3D model (with nuc. pooling)</i>				
EGNN (nuc. pooling)	0.364±0.003	0.619±0.007	0.663±0.010	OOM
SchNet (nuc. pooling)	0.390±0.006	0.685±0.006	0.655±0.038	OOM
FastEGNN (nuc. pooling)	<u>0.444±0.003</u>	<u>0.753±0.015</u>	<u>0.710±0.011</u>	OOM

For detailed descriptions, motivations and significance of the five task settings, please refer to Appendix D.

4 EXPERIMENTS AND RESULTS

4.1 IMPACT OF EXPLICIT GEOMETRY LEARNING ON MODEL PERFORMANCE

We begin by addressing Task 1, where we compare the performance of model families when trained and evaluated on the downstream RNA datasets. Additionally, we provide runtime and memory comparison in Appendix C.

2D models consistently outperform 1D model Results in Table 1 reveal that 2D methods consistently outperform the 1D sequence model across all datasets. Notably, the Transformer1D2D model, which simply augments the attention matrix with adjacency features alongside, achieves around 10% lower prediction MCRMSE on average across datasets than its geometry-free counterpart. This suggests that explicitly incorporating structural information is crucial, as learning from sequence data alone proves to be insufficient. Further experiments, detailed in the Appendix F.4, investigate the learned attention maps of both the Transformer1D2D and the Transformer1D model and their correlation with structural information and reveal that Transformer1D2D attention maps are much more closely aligned with the topological structure of nucleotide graph, reinforcing the conclusion that explicit encoding of structural information is essential for improved performance.

For the foundation models, RNA-FM and SpliceBERT, we observe that for 2 out of 4 datasets (Covid and Ribonanza-2k), RNA foundation models perform worse than the simple supervised transformer baseline whereas for the other two datasets (Tc-Riboswitches and Fungal), transformer and RNA foundation models achieve similar performance. This is consistent with recent works in multiple biology related domains demonstrating specialized foundation models are yet to surpass simple

270 supervised learning baselines (Xu et al., 2024; Kedzierska et al., 2023; Yang et al., 2024). Hence,
271 we choose Transformer1D as the model of choice for subsequent experiments.
272

273
274 **Spectral GNN outperforms spatial GNNs in 2D** ChebNet, a spectral method, outperforms
275 spatial methods such as GCN, GAT, Graph Transformer, and GraphGPS, achieving a prediction
276 MCRMSE 2.5% lower than the next best 2D model across datasets. Spatial GNNs aggregate node
277 features layer by layer, emphasizing local information within a fixed distance. While computation-
278 ally efficient, these methods are limited by the 1-Weisfeiler-Lehman (WL) test, which constrains the
279 expressive power of node-based updates (Xu et al., 2018). In addition, spatial GNNs may suffer from
280 a limited receptive field while spectral methods approximate global graph features, enabling a global
281 receptive field since the first layer. This allows ChebNet to effectively process global information
282 which is important for RNA data due to potential long-range interaction between nucleotides.

283
284 **Challenges of modeling geometric context in all-atom resolution** Contrary to our expectations,
285 3D models at all-atom resolution (EGNN w/o pooling, SchNet w/o pooling [DimeNet \(w/o pooling\)](#),
286 [FAENet \(w/o pooling\)](#), [GVP \(w/o pooling\)](#) and [FastEGNN \(w/o pooling\)](#) in Table 1) show relatively
287 high prediction MCRMSE across datasets, underperforming compared to 1D and 2D methods. We
288 hypothesize this is due to two factors.

289 First, all-atom 3D models rely on a limited local neighborhoods of adjacent atoms, limiting their
290 receptive fields and preventing them from capturing long-range dependencies (see Appendix Ta-
291 ble F.1), which can be crucial for determining RNA properties (Shetty et al., 2013; Alshareedah
292 et al., 2019). Expanding the local neighborhood for these methods turns challenging due to the
293 overwhelming scale of large molecular systems in all-atom resolution. Second, the performance
294 of 3D models is often limited by the inherent inaccuracies in 3D structure prediction tools, which
295 are generally less reliable compared to 2D structure prediction methods (Ponce-Salvatierra et al.,
296 2019). [While FastEGNN is designed for larger molecules, its reliance on the center of mass virtual
297 node initialization may not align well with tasks like RNA property prediction, which inherently
298 have a sequence prior. This may explain the limited performance of FastEGNN in this context and
299 RNA-specific virtual node initialization and carefully designed pooling mechanisms may be needed
300 to further adopt this architecture for large-molecules with a sequence prior.](#)

301 To address the receptive field limitation of all-atom methods, we employ a biological prior by pool-
302 ing atomic features into nucleotide-level representations after a few layers of all-atom operations.
303 This strategy is aligned with RNA’s natural secondary structure, where atoms group into nucleotides,
304 and nucleotides form the complete RNA molecule (Deng et al., 2023). This novel strategy allows
305 us to maintain all-atom resolution in the initial layers while increasing the receptive field via pool-
306 ing. By balancing the number of all-atom and nucleotide layers as hyperparameters, we can balance
307 fine- and coarse-grained all-atom and nucleotide resolution. [Compared to other 3D models, EGNN,
308 FastEGNN and SchNet perform slightly better and hence we introduce the nucleotide pooled vari-
309 ants for these models. We call 3D models with pooling EGNN \(nuc. pooling\), FastEGNN \(nuc.
310 pooling\) and SchNet \(nuc. pooling\). This strategy significantly enhances 3D model performance,
311 reducing prediction MCRMSE by \$\sim 10\%\$ compared to the original EGNN, SchNet, and \[FastEGNN\]\(#\)
312 and outperforming 1D models on the Ribonanza-2k and Tc-Riboswitches datasets by 5% on aver-
313 age. On the COVID dataset, EGNN \(nuc. pooling\) matches the Transformer1D model but still trails
314 behind 2D models. All subsequent experiments report results using nucleotide-pooled versions of
315 the 3D models.](#)

316 Next, we investigated the second hypothesis regarding higher noise in 3D structures by quantifying
317 variability in predicted structures across different 3D prediction tools in Appendix G. We observe
318 substantial variability (between 11-45Å RMSD across structures given by different 3D structure
319 prediction tools), suggesting considerable noise in 3D predictions, which likely contributes to the
320 poorer performance of 3D models.

321 4.2 MODEL EFFICIENCY UNDER LIMITED DATA AND PARTIAL SEQUENCE LABELING

322
323 In this section, we combine the analysis of Tasks 2 and 3, assessing model performance in scenarios
with limited training data or partial labels.

To analyze how the amount of training data influences model performance, we run experiments with varying portions of the full datasets (25%, 50%, 75%, and 100%) on the medium- and large-scale datasets: COVID, Ribonanza-2k, and Fungal (Appendix Fig. 8(a) for illustration). The small size of the Tc-Riboswitches dataset is excluded from the analysis, as training with lower ratios would have resulted in inadequate sample sizes for meaningful evaluation. Additionally, GPU memory constraints prevent the application of Transformer1D2D and 3D models on the Fungal dataset due to its large sequence length.

We also evaluate the impact of partial property labels for nucleotide-level tasks, a common occurrence owing to costly experimental measurements (Wayment-Steele et al., 2020) to identify which models are best suited to handle the challenges of incomplete labels in RNA property prediction. For this, we use the COVID and Ribonanza datasets as these datasets contain nucleotide-level labels. We train the models using all training data but with varying proportions of labeled nucleotides (20%, 40%, 60%, 80%, and 100%) per sequence, thus simulating incomplete or sparse labeling, while testing on fully labeled test sets (Appendix Fig. 8(b) for illustration).

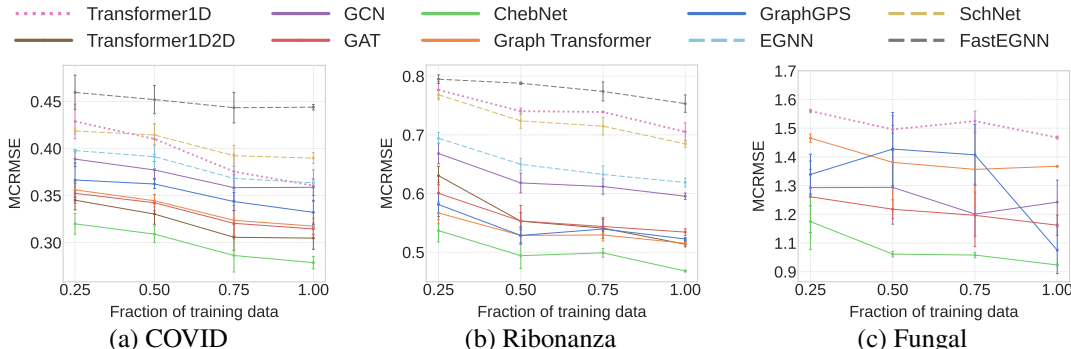


Figure 2: **Performance vs. fraction of training data across various datasets.** Model performance improves with increasing data, with lower MCRMSE across all models. 2D models consistently outperform 1D models, particularly in low-data regimes, underscoring the value of structural information for generalization. Dotted, solid, and dashed lines denote 1D, 2D, and 3D methods, respectively, which applies consistently throughout all figures in this paper.

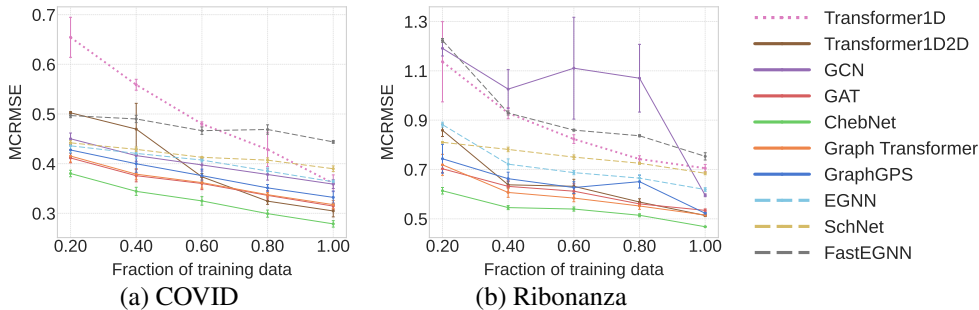


Figure 3: **Performance vs. partial property labels on COVID and Ribonanza datasets.** 2D models consistently outperform 1D models with sparse labeling, while Transformer1D and Transformer1D2D improve rapidly with denser supervision, emphasizing the need for more labels in transformer-based models.

More training data improves performance Unsurprisingly, across all models and datasets, a clear trend emerges: increasing the amount of available data, whether through higher number of training data points or greater proportion of available labels leads to improved performance (Fig. 2, Fig. 3, Appendix Tables in Sec. I.1, I.2). However, the degree of performance improvement varies significantly between model types, as analyzed next.

2D models excel in low data and partial label regimes Evaluating model performance at different training and label ratios reveals a notable trend: 2D models consistently outperform 1D and 3D models under low data and incomplete labeling regimes. Between 20-50% training data and label

levels, 2D models such as ChebNet, Transformer1D2D, GraphGPS, and GAT significantly outperform Transformer1D, highlighting the role of additional structural information for model sample efficiency. Interestingly, Transformer1D and Transformer1D2D exhibit a faster rate of improvement when more labels are available (Fig. 3), suggesting that transformer-based architectures benefit from denser supervision. Notably, Transformer1D requires $2 - 5\times$ more training data/labels to match the performance of the least effective 2D models, which achieve comparable results using only 20% to 50% of the training data needed by Transformer1D when trained on the full dataset.

3D models outperform 1D model in limited data regime despite structural noise For the medium-scale datasets (COVID and Ribonanza), where 3D models can be evaluated, we observe that the 3D models generally outperform or are on par with the Transformer1D, even for lower data and labeling regimes. This suggests that despite the noise introduced by inaccuracies in 3D structure predictions, the explicit geometric encoding in 3D models still provides an advantage over 1D models. EGNN, in particular, is consistently better than or on par with Transformer1D across all training and label ratios. This further emphasizes that models incorporating explicit geometric encoding (whether 2D or 3D) are more data-efficient than those relying solely on sequence information. However, it is important to note that 3D models do not match the efficiency of 2D models in these scenarios, likely due to their susceptibility to noise as discussed in Section 4.1.

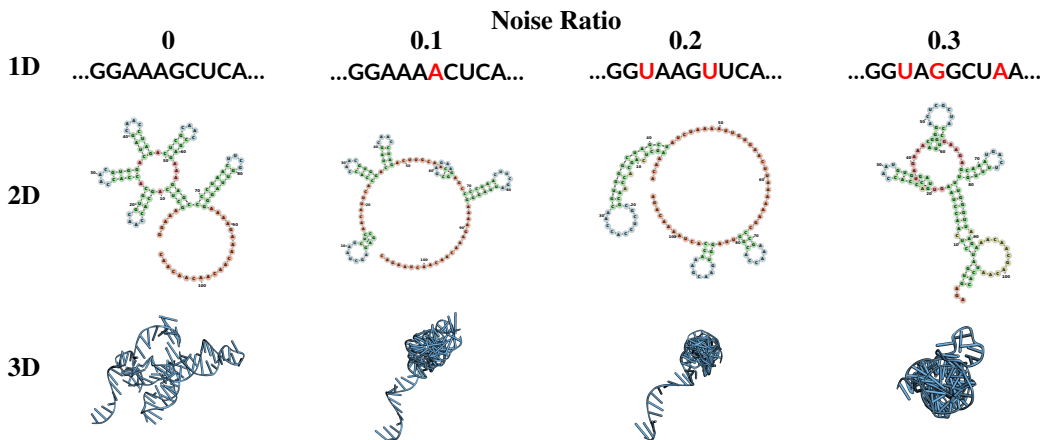


Figure 4: **Visualization of 1D, 2D, and 3D structures under varying noise ratios (mutation errors during sequencing).** Each column represents a different noise ratio, showcasing the impact of noise on the structures across different dimensions.

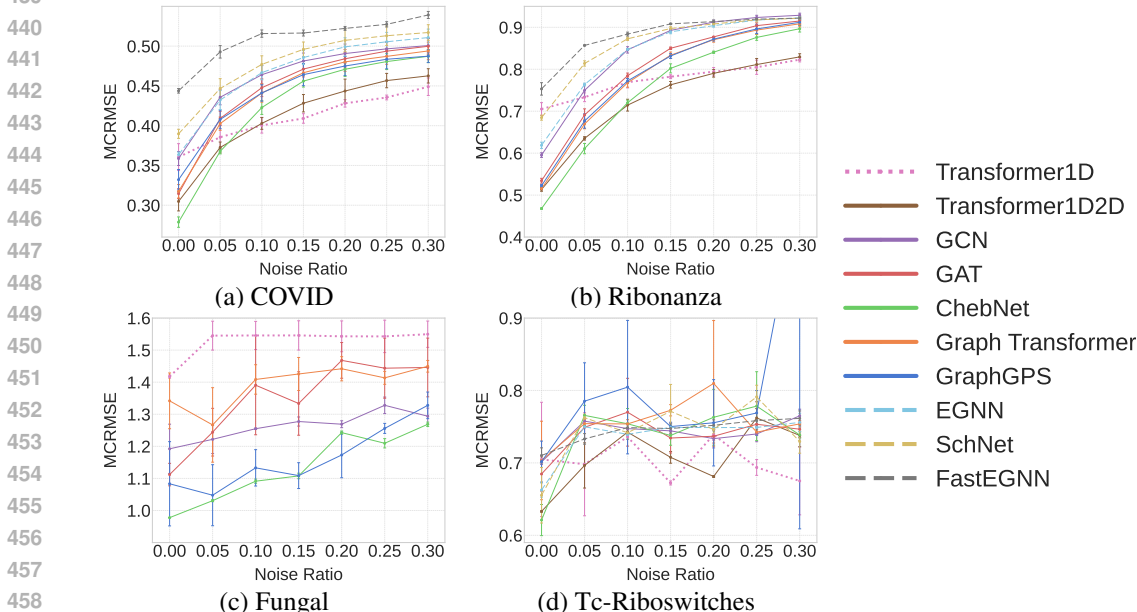
4.3 MODEL ROBUSTNESS AND GENERALIZATION UNDER SEQUENCING NOISE

Tasks 4 and 5 both deal with model performance with noise in the data, but focus on different aspects, robustness to noise, and ability to generalize across unseen noise distributions. As explained in Sec. 3, sequencing noise is common depending on the sequencing method and platform used (Fox et al., 2014), thereby introducing errors in sequences that propagate into 2D and 3D structures. Additionally one of the deployment scenarios involves models trained on high-quality clean data applied for datasets acquired under noisy conditions owing to different sequencing platforms or experimental batch effects (Tom et al., 2017).

To explore these practical aspects, we design two sets of experiments:

- *Robustness:* We introduce sequencing noise into the training, validation, and test sequences to simulate realistic sequencing errors. Nucleotide mutations are applied with probabilities $\{0.05, 0.1, 0.15, 0.2, 0.25, 0.3\}$, mirroring typical sequencing error rates (Pfeiffer et al., 2018) which also propagates to the 2D and 3D structures (Fig. 4) via structure prediction tools. Importantly, these mutations are not random; the likelihood of a particular nucleotide mutating into another varies, as is well documented in sequencing studies Pfeiffer et al. (2018). Our noise model reflects these real-world mutation profiles. Crucially, while the input training, validation, and test sequences contain

432 noise, the property labels remain clean. This again reflects practical scenarios where labels are
 433 experimentally determined independent of sequencing and thus unaffected by sequencing errors.
 434
 435 • *Generalization:* Here, models are trained on clean, noise-free data corresponding to high-quality
 436 sequencing experiments but are tested on datasets with varying levels of noise simulated by se-
 437 quencing mutation probabilities in $\{0.05, 0.1, 0.15, 0.2, 0.25, 0.3\}$. This setup reflects the real-
 438 world scenario where models trained on high-quality data will be deployed on OOD data that may
 439 come from different sequencers or have been affected by batch effects.



459 **Figure 5: Robustness experiments.** Transformer1D shows the least performance drop under in-
 460 creasing noise, maintaining the highest accuracy, with Transformer1D2D following closely. In con-
 461 trast, 2D and 3D models, particularly ChebNet and 3D models, are more impacted by noise.
 462

463 **Transformer architectures demonstrate superior robustness and generalization under se-**
 464 **quencing noise** Expectedly, across both tasks, increased noise levels generally leads to worse
 465 test MCRMSE for all models, indicating a decline in prediction performance (Fig. 5, Fig. 6 and
 466 Appendix Tables in Sec. I.3, I.4).
 467

468 Among all models, Transformer1D demonstrates the highest robustness and generalization, exhibit-
 469 ing the least performance degradation as noise levels increase. Notably, in generalization exper-
 470 iments, Transformer1D achieves the best prediction MCRMSE on the COVID, Ribonanza, and
 471 Tc-Riboswitches datasets under higher noise levels (Fig. 6 and Appendix I.4). The reliance of
 472 Transformer1D on sequence-only information without considering geometric context, while being
 473 a weakness in other scenarios, becomes a strength in case of noisy sequences as minor sequenc-
 474 ing errors may severely alter the predicted RNA structures (Fig. 4). While its performance on the
 475 Fungal dataset is worse overall, Transformer1D maintains remarkably consistent performance as
 476 noise increases. Transformer1D2D ranks just behind Transformer1D outperforming other 2D and
 477 3D models. This can be attributed to Transformer1D2D’s ability to selectively focus on sequence
 478 information for noisy data rather than relying on structural data alone as the self-attention is only
 weakly conditioned on the graph topology.

479 More elaborated 2D and 3D models, which rigidly rely on structural information, are significantly
 480 more affected by noise, underperforming compared to plain sequence baseline in both robustness
 481 and generalization experiments for high noise levels. For low-to-moderate noise levels (5-10%
 482 noise), 2D methods such as ChebNet still perform the best. Interestingly, ChebNet shows the worst
 483 generalization among 2D models, although it performs on par with other methods in robustness
 484 experiments. This suggests that while ChebNet struggles with OOD noise, its performance gets
 485 better when it is also trained on the same noise level used during testing, highlighting the need
 for retraining for different experimental data batches/noise levels in real-world applications. Across

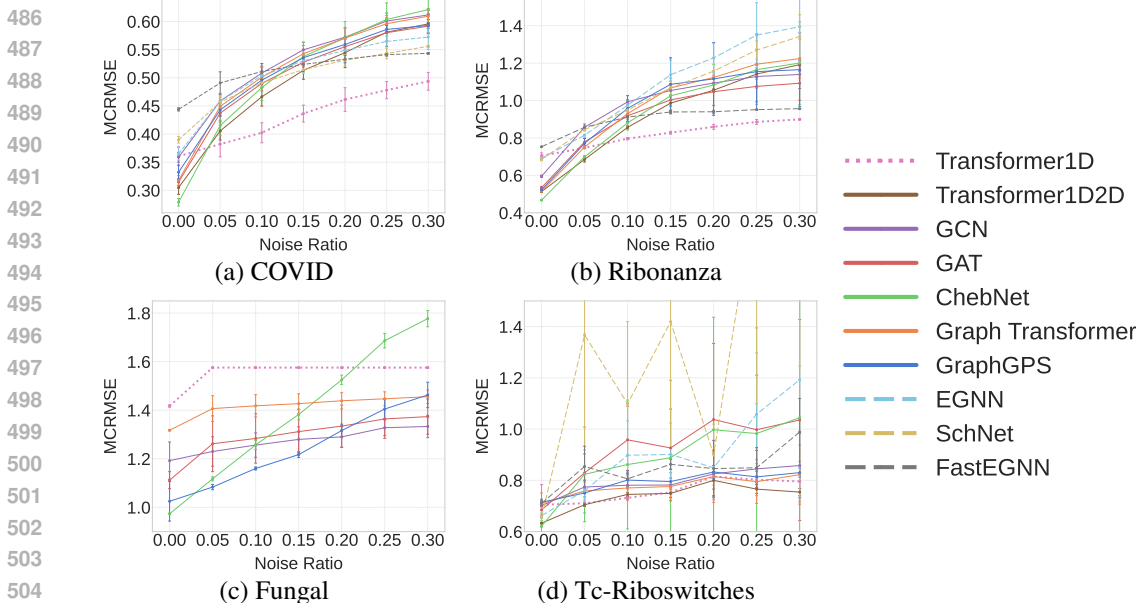


Figure 6: **Generalization experiments.** Transformer1D outperforms other models on noisy sequences, achieving the lowest RMSE at higher noise levels, particularly on COVID, Ribonanza, and Tc-Riboswitches. Transformer1D2D follows closely, showing that transformer-based models generalize better under noise than 2D and 3D models, especially in tasks with geometric representations.

both experiments, 3D models have poor performance for more noisy conditions, particularly with the COVID and Ribonanza datasets, due to their dependence on 3D structures which are also sensitive to the propagation of sequencing errors (Fig.4 bottom). In the smaller Tc-Riboswitches dataset, model performances vary more, likely due to limited data size, but transformer models still consistently demonstrate greater robustness to noise.

Across both settings, as the noise ratio rises, the 1D model demonstrates the greatest resilience to noise, showing an average test MCRMSE increase of approximately 14% and 27%, respectively, relative to the train and test on clean data. In contrast, 2D models exhibit the highest sensitivity, with test MCRMSE increasing from 30% to 82%. Meanwhile, 3D models show intermediate performance, with MCRMSE increases of 29% and 56%. Our results reveal a higher vulnerability of 2D and 3D models to sequencing noise where geometric context becomes unreliable at a faster rate than a plain sequence of nucleotides.

5 CONCLUSION

We present the first comprehensive study on the benefits and challenges of the effect of geometric context for RNA property prediction models. With providing a curated set of RNA datasets with annotated 2D and 3D structures, we systematically evaluate the performance of 1D, 2D, and 3D models under various real-world conditions, such as limited data, partial labeling, sequencing errors and out-of-distribution generalization. Our results reveal that 2D models outperform 1D and 3D models, with spectral graph neural networks excelling even in low-data and partial labeling scenarios. For 3D models, we find that their potential benefits are hindered by the limited receptive field, computational complexity, and structural noise from RNA structure prediction tools. At the same time, 1D models demonstrate better robustness compared to 2D and 3D models in noisy and OOD conditions. This study highlights the value and limitations of using geometric context for RNA modeling. Future work could focus on ensembling 1D, 2D, and 3D models for complementary strengths, and on improving 2D and 3D models to better handle noise from structure prediction tools as elaborated in Appendix E.2. Another promising direction can be to investigate advanced 3D model architectures which incorporate high-degree steerable features as discussed in Appendix E.1.

ETHICS STATEMENT

This work aims to advance the computational prediction of RNA properties through the development and evaluation of machine learning models utilizing diverse representations of RNA, including 1D sequences, 2D structures, and 3D geometries. In conducting this research, we are committed to upholding high ethical standards in all aspects of our study, ensuring that our work promotes scientific integrity, transparency, and responsible use of technology.

- **Data Integrity and Fair Use:** All RNA datasets used in this study were acquired from publicly available and ethically sourced repositories. Where applicable, the original data sources have been duly cited, and all efforts have been made to ensure data privacy and compliance with relevant data-sharing agreements. Our curated datasets have been handled responsibly, with proper annotations to minimize errors and misinterpretations.
- **Minimization of Bias:** We recognize that RNA data, particularly when it involves limited or incomplete datasets, can introduce biases in model predictions. To mitigate this, we employ a diverse set of RNA data and systematically analyze model performance under various conditions, including label scarcity and sequencing errors. By doing so, we aim to provide balanced insights into the potential advantages and limitations of different modeling approaches, fostering responsible model selection and deployment.
- **Responsible Use of AI in Biology:** The machine learning techniques used in this study are intended to assist in scientific discovery and biological understanding, with potential applications in therapeutic interventions. However, we acknowledge the importance of caution in applying computational models in sensitive domains such as healthcare. While our models are designed to improve RNA property prediction, we emphasize that these predictions should not be used in isolation for clinical or therapeutic decision-making without further validation and consideration of ethical implications.

REPRODUCIBILITY STATEMENT

We are committed to the transparency and reproducibility of our findings. All methodologies, datasets, and benchmarking environments will be made publicly available to the research community, allowing others to reproduce, verify, and extend our work. This open approach aims to advance the field of RNA research and promote collaborative progress. To ensure reproducibility, we also provide detailed descriptions of model architecture and training procedures in the main text. The appendix H contains full details on data preprocessing, hyperparameter searching and additional experimental information. All data and code will be provided to upon acceptance.

REFERENCES

- Takuya Akiba, Shotaro Sano, Toshihiko Yanase, Takeru Ohta, and Masanori Koyama. Optuna: A next-generation hyperparameter optimization framework. In *Proceedings of the 25th ACM SIGKDD international conference on knowledge discovery & data mining*, pp. 2623–2631, 2019.
- Juan D Alfonzo, Jessica A Brown, Peter H Byers, Vivian G Cheung, Richard J Maraia, and Robert L Ross. A call for direct sequencing of full-length rnas to identify all modifications. *Nature genetics*, 53(8):1113–1116, 2021.
- Ibraheem Alshareedah, Taranpreet Kaur, Jason Ngo, Hannah Seppala, Liz-Audrey Djomnang Kounatse, Wei Wang, Mahdi Muhammad Moosa, and Priya R Banerjee. Interplay between short-range attraction and long-range repulsion controls reentrant liquid condensation of ribonucleoprotein–rna complexes. *Journal of the American Chemical Society*, 141(37):14593–14602, 2019.
- Viplove Arora and Guido Sanguinetti. De novo prediction of rna–protein interactions with graph neural networks. *RNA*, 28(11):1469–1480, 2022.
- Minkyung Baek, Ryan McHugh, Ivan Anishchenko, Hanlun Jiang, David Baker, and Frank DiMaio. Accurate prediction of protein–nucleic acid complexes using rosettafoldna. *Nature methods*, 21(1):117–121, 2024.

- 594 Ilyes Batatia, David P Kovacs, Gregor Simm, Christoph Ortner, and Gábor Csányi. Mace: Higher
595 order equivariant message passing neural networks for fast and accurate force fields. *Advances in*
596 *Neural Information Processing Systems*, 35:11423–11436, 2022.
- 597 Simon Batzner, Albert Musaelian, Lixin Sun, Mario Geiger, Jonathan P Mailoa, Mordechai Ko-
598 rnlbluth, Nicola Molinari, Tess E Smidt, and Boris Kozinsky. E (3)-equivariant graph neural
599 networks for data-efficient and accurate interatomic potentials. *Nature communications*, 13(1):
600 2453, 2022.
- 601 Michal J Boniecki, Grzegorz Lach, Wayne K Dawson, Konrad Tomala, Pawel Lukasz, Tomasz
602 Soltysinski, Kristian M Rother, and Janusz M Bujnicki. Simrna: a coarse-grained method for rna
603 folding simulations and 3d structure prediction. *Nucleic acids research*, 44(7):e63–e63, 2016.
- 604 Sara A Byron, Kendall R Van Keuren-Jensen, David M Engelthaler, John D Carpten, and David W
605 Craig. Translating rna sequencing into clinical diagnostics: opportunities and challenges. *Nature*
606 *Reviews Genetics*, 17(5):257–271, 2016.
- 607 Jiacheng Cen, Anyi Li, Ning Lin, Yuxiang Ren, Zihe Wang, and Wenbing Huang. Are high-
608 degree representations really unnecessary in equivariant graph neural networks? *arXiv preprint*
609 *arXiv:2410.11443*, 2024.
- 610 Jiayang Chen, Zhihang Hu, Siqi Sun, Qingxiong Tan, Yixuan Wang, Qinze Yu, Licheng Zong, Liang
611 Hong, Jin Xiao, Tao Shen, et al. Interpretable rna foundation model from unannotated data for
612 highly accurate rna structure and function predictions. *arXiv preprint arXiv:2204.00300*, 2022.
- 613 Ken Chen, Yue Zhou, Maolin Ding, Yu Wang, Zhixiang Ren, and Yuedong Yang. Self-supervised
614 learning on millions of pre-mrna sequences improves sequence-based rna splicing prediction.
615 *bioRxiv*, pp. 2023–01, 2023.
- 616 Xinshi Chen, Yu Li, Ramzan Umarov, Xin Gao, and Le Song. Rna secondary structure prediction
617 by learning unrolled algorithms. *arXiv preprint arXiv:2002.05810*, 2020.
- 618 Rhiju Das and David Baker. Automated de novo prediction of native-like rna tertiary structures.
619 *Proceedings of the National Academy of Sciences*, 104(37):14664–14669, 2007.
- 620 Michaël Defferrard, Xavier Bresson, and Pierre Vandergheynst. Convolutional neural networks
621 on graphs with fast localized spectral filtering. In *Advances in Neural Information Processing*
622 *Systems*, pp. 3844–3852, 2016.
- 623 Jie Deng, Xianyang Fang, Lin Huang, Shanshan Li, Lilei Xu, Keqiong Ye, Jinsong Zhang, Kaiming
624 Zhang, and Qiangfeng Cliff Zhang. Rna structure determination: From 2d to 3d. *Fundamental*
625 *Research*, 3(5):727–737, 2023.
- 626 Alexandre Agm Duval, Victor Schmidt, Alex Hernández-García, Santiago Miret, Fragkiskos D
627 Malliaros, Yoshua Bengio, and David Rolnick. Faenet: Frame averaging equivariant gnn for
628 materials modeling. In *International Conference on Machine Learning*, pp. 9013–9033. PMLR,
629 2023.
- 630 Matthias Fey and Jan E. Lenssen. Fast graph representation learning with PyTorch Geometric. In
631 *ICLR Workshop on Representation Learning on Graphs and Manifolds*, 2019.
- 632 Edward J Fox, Kate S Reid-Bayliss, Mary J Emond, and Lawrence A Loeb. Accuracy of next
633 generation sequencing platforms. *Next generation, sequencing & applications*, 1, 2014.
- 634 J Thorben Frank, Oliver T Unke, Klaus-Robert Müller, and Stefan Chmiela. A euclidean transformer
635 for fast and stable machine learned force fields. *Nature Communications*, 15(1):6539, 2024.
- 636 Jörg Franke, Frederic Runge, and Frank Hutter. Probabilistic transformer: Modelling ambiguities
637 and distributions for rna folding and molecule design. *Advances in Neural Information Processing*
638 *Systems*, 35:26856–26873, 2022.
- 639 Laiyi Fu, Yingxin Cao, Jie Wu, Qinke Peng, Qing Nie, and Xiaohui Xie. Ufold: fast and accurate
640 rna secondary structure prediction with deep learning. *Nucleic acids research*, 50(3):e14–e14,
641 2022.

- 648 Johannes Gasteiger, Janek Groß, and Stephan Günnemann. Directional message passing for molec-
649 ular graphs. *arXiv preprint arXiv:2003.03123*, 2020.
- 650
- 651 Ann-Christin Groher, Sven Jager, Christopher Schneider, Florian Groher, Kay Hamacher, and Beat-
652 rix Suess. Tuning the performance of synthetic riboswitches using machine learning. *ACS syn-
653 thetic biology*, 8(1):34–44, 2018.
- 654
- 655 Jiaqi Han, Yu Rong, Tingyang Xu, and Wenbing Huang. Geometrically equivariant graph neural
656 networks: A survey. *arXiv preprint arXiv:2202.07230*, 2022.
- 657
- 658 Yixing Han, Shouguo Gao, Kathrin Muegge, Wei Zhang, and Bing Zhou. Advanced applications of
659 rna sequencing and challenges. *Bioinformatics and biology insights*, 9:BBI–S28991, 2015.
- 660
- 661 Shujun He, Baizhen Gao, Rushant Sabnis, and Qing Sun. Nucleic transformer: Deep learning on
662 nucleic acids with self-attention and convolutions. *bioRxiv*, pp. 2021–01, 2021.
- 663
- 664 Shujun He, Baizhen Gao, Rushant Sabnis, and Qing Sun. Rnadegformer: accurate prediction of
665 mrna degradation at nucleotide resolution with deep learning. *Briefings in Bioinformatics*, 24(1):
666 bbac581, 2023.
- 667
- 668 Shujun He, Rui Huang, Jill Townley, Rachael C Kretsch, Thomas G Karagianes, David BT Cox,
669 Hamish Blair, Dmitry Penzar, Valeriy Vyaltsev, Elizaveta Aristova, et al. Ribonanza: deep learn-
670 ing of rna structure through dual crowdsourcing. *bioRxiv*, 2024.
- 671
- 672 Ivo L Hofacker, Walter Fontana, Peter F Stadler, L Sebastian Bonhoeffer, Manfred Tacker, Peter
673 Schuster, et al. Fast folding and comparison of rna secondary structures. *Monatshfte fur chemie*,
674 125:167–167, 1994.
- 675
- 676 Shion Honda, Shoi Shi, and Hiroki R Ueda. Smiles transformer: Pre-trained molecular fingerprint
677 for low data drug discovery. *arXiv preprint arXiv:1911.04738*, 2019.
- 678
- 679 Bowen Jing, Stephan Eismann, Patricia Suriana, Raphael JL Townshend, and Ron Dror. Learning
680 from protein structure with geometric vector perceptrons. *arXiv preprint arXiv:2009.01411*, 2020.
- 681
- 682 Chaitanya K. Joshi, Cristian Bodnar, Simon V. Mathis, Taco Cohen, and Pietro Liò. On the ex-
683 pressive power of geometric graph neural networks. In *International Conference on Machine
684 Learning*, 2023.
- 685
- 686 Wolfgang Kabsch. A solution for the best rotation to relate two sets of vectors. *Acta Crystallo-
687 graphica Section A: Crystal Physics, Diffraction, Theoretical and General Crystallography*, 32
688 (5):922–923, 1976.
- 689
- 690 Kasia Z Kedzierska, Lorin Crawford, Ava P Amini, and Alex X Lu. Assessing the limits of zero-shot
691 foundation models in single-cell biology. *bioRxiv*, pp. 2023–10, 2023.
- 692
- 693 Thomas N Kipf and Max Welling. Semi-supervised classification with graph convolutional net-
694 works. In *5th International Conference on Learning Representations, ICLR 2017, Toulon, France,
695 April 24-26, 2017, Conference Track Proceedings*, 2017.
- 696
- 697 Boris Knyazev, Xiao Lin, Mohamed R Amer, and Graham W Taylor. Spectral multigraph networks
698 for discovering and fusing relationships in molecules. *arXiv preprint arXiv:1811.09595*, 2018.
- 699
- 700 Sowmya R Krishnan, Arijit Roy, and M Michael Gromiha. Reliable method for predicting the
701 binding affinity of rna-small molecule interactions using machine learning. *Briefings in Bioinfor-
matics*, 25(2):bbac002, 2024.
- Mandar Kulkarni, Jayaraman Thangappan, Indrajit Deb, and Sangwook Wu. Comparative analysis
of rna secondary structure accuracy on predicted rna 3d models. *Plos one*, 18(9):e0290907, 2023.
- Han Li, Dan Zhao, and Jianyang Zeng. Kpgt: knowledge-guided pre-training of graph transformer
for molecular property prediction. In *Proceedings of the 28th ACM SIGKDD Conference on
Knowledge Discovery and Data Mining*, pp. 857–867, 2022.

- 702 Chandran Nithin, Sebastian Kmiecik, Roman Błaszczuk, Julita Nowicka, and Irina Tuszyńska. Com-
703 parative analysis of rna 3d structure prediction methods: towards enhanced modeling of rna-
704 ligand interactions. *Nucleic Acids Research*, 52(13):7465–7486, 2024.
- 705
706 Fatih Ozsolak and Patrice M Milos. Rna sequencing: advances, challenges and opportunities. *Nature*
707 *reviews genetics*, 12(2):87–98, 2011.
- 708 Robin Pearce, Gilbert S Omenn, and Yang Zhang. De novo rna tertiary structure prediction at atomic
709 resolution using geometric potentials from deep learning. *BioRxiv*, pp. 2022–05, 2022.
- 710
711 Rafael Josip Penić, Tin Vlašić, Roland G Huber, Yue Wan, and Mile Šikić. Rinalmo: General-
712 purpose rna language models can generalize well on structure prediction tasks. *arXiv preprint*
713 *arXiv:2403.00043*, 2024.
- 714 Franziska Pfeiffer, Carsten Gröber, Michael Blank, Kristian Händler, Marc Beyer, Joachim L
715 Schultze, and Günter Mayer. Systematic evaluation of error rates and causes in short samples
716 in next-generation sequencing. *Scientific reports*, 8(1):10950, 2018.
- 717
718 Almudena Ponce-Salvatierra, Astha, Katarzyna Merdas, Chandran Nithin, Pritha Ghosh, Sunan-
719 dan Mukherjee, and Janusz M Bujnicki. Computational modeling of rna 3d structure based on
720 experimental data. *Bioscience reports*, 39(2):BSR20180430, 2019.
- 721 Ladislav Rampášek, Mikhail Galkin, Vijay Prakash Dwivedi, Anh Tuan Luu, Guy Wolf, and Do-
722 minique Beaini. Recipe for a General, Powerful, Scalable Graph Transformer. *Advances in Neural*
723 *Information Processing Systems*, 35, 2022.
- 724
725 Ugur Sahin, Katalin Karikó, and Özlem Türeci. mrna-based therapeutics—developing a new class
726 of drugs. *Nature reviews Drug discovery*, 13(10):759–780, 2014.
- 727 Victor Garcia Satorras, Emiel Hoogeboom, and Max Welling. E (n) equivariant graph neural net-
728 works. In *International conference on machine learning*, pp. 9323–9332. PMLR, 2021.
- 729
730 Tamar Schlick and Anna Marie Pyle. Opportunities and challenges in rna structural modeling and
731 design. *Biophysical journal*, 113(2):225–234, 2017.
- 732
733 Bohdan Schneider, Blake Alexander Sweeney, Alex Bateman, Jiri Cerny, Tomasz Zok, and Marta
734 Szachniuk. When will rna get its alphafold moment? *Nucleic Acids Research*, 51(18):9522–9532,
2023.
- 735
736 Kristof Schütt, Pieter-Jan Kindermans, Huziel Enoc Saucedo Felix, Stefan Chmiela, Alexandre
737 Tkatchenko, and Klaus-Robert Müller. Schnet: A continuous-filter convolutional neural network
738 for modeling quantum interactions. *Advances in neural information processing systems*, 30, 2017.
- 739
740 Shantanu Sharma, Feng Ding, and Nikolay V Dokholyan. ifoldrna: three-dimensional rna structure
prediction and folding. *Bioinformatics*, 24(17):1951–1952, 2008.
- 741
742 Phillip A Sharp. The centrality of rna. *Cell*, 136(4):577–580, 2009.
- 743
744 Tao Shen, Zhihang Hu, Zhangzhi Peng, Jiayang Chen, Peng Xiong, Liang Hong, Liangzhen Zheng,
745 Yixuan Wang, Irwin King, Sheng Wang, et al. E2efold-3d: End-to-end deep learning method for
accurate de novo rna 3d structure prediction. *arXiv preprint arXiv:2207.01586*, 2022.
- 746
747 Sumangala Shetty, Snezana Stefanovic, and Mihaela Rita Mihailescu. Hepatitis c virus rna: molec-
748 ular switches mediated by long-range rna–rna interactions? *Nucleic acids research*, 41(4):2526–
2540, 2013.
- 749
750 Yunsheng Shi, Zhengjie Huang, Shikun Feng, Hui Zhong, Wenjin Wang, and Yu Sun. Masked label
751 prediction: Unified message passing model for semi-supervised classification. *arXiv preprint*
752 *arXiv:2009.03509*, 2020.
- 753
754 Jaswinder Singh, Kuldip Paliwal, Tongchuan Zhang, Jaspreet Singh, Thomas Litfin, and Yaoqi
755 Zhou. Improved rna secondary structure and tertiary base-pairing prediction using evolution-
ary profile, mutational coupling and two-dimensional transfer learning. *Bioinformatics*, 37(17):
2589–2600, 2021.

- 756 Necla Nisa Soylu and Emre Sefer. Bert2ome: Prediction of 2-o-methylation modifications from rna
757 sequence by transformer architecture based on bert. *IEEE/ACM Transactions on Computational*
758 *Biology and Bioinformatics*, 20(3):2177–2189, 2023.
- 759 Eric J Strobel, Kyle E Watters, David Loughrey, and Julius B Lucks. Rna systems biology: uniting
760 functional discoveries and structural tools to understand global roles of rnas. *Current opinion in*
761 *biotechnology*, 39:182–191, 2016.
- 762 Marc Teufel and Patrick Sobetzko. Reducing costs for dna and rna sequencing by sample pooling
763 using a metagenomic approach. *BMC genomics*, 23(1):613, 2022.
- 764 Nathaniel Thomas, Tess Smidt, Steven Kearnes, Lusann Yang, Li Li, Kai Kohlhoff, and Patrick
765 Riley. Tensor field networks: Rotation-and translation-equivariant neural networks for 3d point
766 clouds. *arXiv preprint arXiv:1802.08219*, 2018.
- 767 Jennifer A Tom, Jens Reeder, William F Forrest, Robert R Graham, Julie Hunkapiller, Timothy W
768 Behrens, and Tushar R Bhangale. Identifying and mitigating batch effects in whole genome
769 sequencing data. *BMC bioinformatics*, 18:1–12, 2017.
- 770 Hoa Thi Nhu Tran, Kok Siong Ang, Marion Chevrier, Xiaomeng Zhang, Nicole Yee Shin Lee,
771 Michelle Goh, and Jinmiao Chen. A benchmark of batch-effect correction methods for single-cell
772 rna sequencing data. *Genome biology*, 21:1–32, 2020.
- 773 Ashish Vaswani, Noam Shazeer, Niki Parmar, Jakob Uszkoreit, Llion Jones, Aidan N Gomez,
774 Łukasz Kaiser, and Illia Polosukhin. Attention is all you need. In *Advances in Neural Infor-*
775 *mation Processing Systems*, pp. 5998–6008, 2017.
- 776 Petar Veličković, Guillem Cucurull, Arantxa Casanova, Adriana Romero, Pietro Liò, and Yoshua
777 Bengio. Graph attention networks. In *6th International Conference on Learning Representations,*
778 *ICLR 2018, Vancouver, BC, Canada, April 30–May 3, 2018, Conference Track Proceedings*, 2018.
- 779 Hong Wang, Shuyu Wang, Yong Zhang, Shoudong Bi, and Xiaolei Zhu. A brief review of machine
780 learning methods for rna methylation sites prediction. *Methods*, 203:399–421, 2022.
- 781 Wenkai Wang, Chenjie Feng, Renmin Han, Ziyi Wang, Lisha Ye, Zongyang Du, Hong Wei,
782 Fa Zhang, Zhenling Peng, and Jianyi Yang. ttrasettarna: automated prediction of rna 3d structure
783 with transformer network. *Nature Communications*, 14(1):7266, 2023.
- 784 Hannah K. Wayment-Steele, Wipapat Kladwang, and Rhiju Das. Rna secondary structure packages
785 ranked and improved by high-throughput experiments. *bioRxiv*, 2020. doi: 10.1101/2020.05.29.
786 124511. URL <https://www.biorxiv.org/content/early/2020/05/31/2020.05.29.124511>.
- 787 Hannah K Wayment-Steele, Wipapat Kladwang, Alexandra I Strom, Jeehyung Lee, Adrien Treuille,
788 Alex Becka, Eterna Participants, and Rhiju Das. Rna secondary structure packages evaluated and
789 improved by high-throughput experiments. *Nature methods*, 19(10):1234–1242, 2022a.
- 790 Hannah K Wayment-Steele, Wipapat Kladwang, Andrew M Watkins, Do Soon Kim, Bojan Tunguz,
791 Walter Reade, Maggie Demkin, Jonathan Romano, Roger Wellington-Oguri, John J Nicol, et al.
792 Deep learning models for predicting rna degradation via dual crowdsourcing. *Nature Machine*
793 *Intelligence*, 4(12):1174–1184, 2022b.
- 794 Oliver Wieder, Stefan Kohlbacher, Méline Kuenemann, Arthur Garon, Pierre Ducrot, Thomas Sei-
795 del, and Thierry Langer. A compact review of molecular property prediction with graph neural
796 networks. *Drug Discovery Today: Technologies*, 37:1–12, 2020.
- 797 Rhondene Wint, Asaf Salamov, and Igor V Grigoriev. Kingdom-wide analysis of fungal protein-
798 coding and trna genes reveals conserved patterns of adaptive evolution. *Molecular biology and*
799 *evolution*, 39(2):msab372, 2022.
- 800 Keyulu Xu, Weihua Hu, Jure Leskovec, and Stefanie Jegelka. How powerful are graph neural
801 networks? In *International Conference on Learning Representations*, 2018.

- 810 Xiaojun Xu, Peinan Zhao, and Shi-Jie Chen. Vfold: a web server for rna structure and folding
811 thermodynamics prediction. *PLoS one*, 9(9):e107504, 2014.
- 812
- 813 Zongzhe Xu, Ritvik Gupta, Wenduo Cheng, Alexander Shen, Junhong Shen, Ameet Talwalkar, and
814 Mikhail Khodak. Specialized foundation models struggle to beat supervised baselines. *arXiv*
815 *preprint arXiv:2411.02796*, 2024.
- 816 Zichao Yan, William L Hamilton, and Mathieu Blanchette. Graph neural representational learn-
817 ing of rna secondary structures for predicting rna-protein interactions. *Bioinformatics*, 36
818 (Supplement_1):i276–i284, 2020.
- 819
- 820 Kevin K Yang, Nicolo Fusi, and Alex X Lu. Convolutions are competitive with transformers for
821 protein sequence pretraining. *Cell Systems*, 15(3):286–294, 2024.
- 822
- 823 Yuning Yang, Gen Li, Kuan Pang, Wuxinhao Cao, Xiangtao Li, and Zhaolei Zhang. Deciphering
824 3’utr mediated gene regulation using interpretable deep representation learning. *bioRxiv*, pp.
825 2023–09, 2023.
- 826
- 827 Xian-bin Ye, Quanlong Guan, Weiqi Luo, Liangda Fang, Zhao-Rong Lai, and Jun Wang. Molecu-
828 lar substructure graph attention network for molecular property identification in drug discovery.
Pattern Recognition, 128:108659, 2022.
- 829
- 830 Yi Zhang, Jun Wang, and Yi Xiao. 3drna: Building rna 3d structure with improved template library.
Computational and structural biotechnology journal, 18:2416–2423, 2020.
- 831
- 832 Yuelin Zhang, Jiacheng Cen, Jiaqi Han, Zhiqiang Zhang, Jun Zhou, and Wenbing Huang. Improving
833 equivariant graph neural networks on large geometric graphs via virtual nodes learning. In *Forty-*
834 *first International Conference on Machine Learning*.
- 835
- 836 Jingjing Zheng, Yurong Qian, Jie He, Zerui Kang, and Lei Deng. Graph neural network with self-
837 supervised learning for noncoding rna–drug resistance association prediction. *Journal of Chemi-
cal Information and Modeling*, 62(15):3676–3684, 2022.
- 838
- 839 Jinhua Zhu, Yingce Xia, Lijun Wu, Shufang Xie, Wengang Zhou, Tao Qin, Houqiang Li, and Tie-
840 Yan Liu. Dual-view molecular pre-training. In *Proceedings of the 29th ACM SIGKDD Conference*
841 *on Knowledge Discovery and Data Mining*, pp. 3615–3627, 2023.
- 842
- 843
- 844
- 845
- 846
- 847
- 848
- 849
- 850
- 851
- 852
- 853
- 854
- 855
- 856
- 857
- 858
- 859
- 860
- 861
- 862
- 863

APPENDIX OVERVIEW

- **Appendix A:** Related Work.
- **Appendix B:** Models Overview.
- **Appendix C:** Memory and Computational Constraints.
- **Appendix D:** Detailed task descriptions.
- **Appendix E:** Discussion on Advanced Model Architectures.
- **Appendix F:** Additional Experimental Information.
- **Appendix G:** Analysis of Noise in 3D Structures.
- **Appendix H:** Reproduction.
- **Appendix I:** Additional Results.

A RELATED WORK

RNA property prediction RNA-specific models remain scarce, likely due to limited specialized datasets. Recent advancements in sequence modeling have shown promise, particularly with foundation models like RNA-FM (Chen et al., 2022), UTRBERT (Yang et al., 2023), and RINALMO (Penić et al., 2024), which use transformer-based architectures pre-trained on large RNA sequence corpora to predict various RNA functions and structures. While RNNs and CNNs have been applied to tasks like RNA methylation and protein binding (Wang et al., 2022), they struggle with long-range dependencies. Hybrid models like RNAdegformer (He et al., 2023), combining convolutional layers with self-attention, improve predictions by capturing both local and global dependencies. Although some efforts integrate 2D structures with transformers, explicit 2D and 3D geometric modeling for RNA remains underexplored, with graph-based models mainly focusing on RNA-protein and RNA-drug interaction tasks rather than property prediction (Krishnan et al., 2024; Yan et al., 2020; Arora & Sanguinetti, 2022; Zheng et al., 2022).

RNA structure prediction RNA 2D structure prediction has progressed from dynamic programming methods like Vienna RNAfold (Hofacker et al., 1994) to deep learning-based tools like SPOT-RNA2 (Singh et al., 2021) and Ufold (Fu et al., 2022), which enhance accuracy by using neural networks and evolutionary data. Models such as E2Efold (Chen et al., 2020) and RNA-FM (Chen et al., 2022) employ transformer architectures to achieve state-of-the-art results in secondary structure prediction.

RNA 3D structure prediction has progressed through ab initio, template-based, and deep learning approaches. Ab initio methods (e.g., iFoldRNA (Sharma et al., 2008), SimRNA (Boniecki et al., 2016)) balance detail and efficiency but struggle with non-canonical interactions. Template-based models (e.g., FARNA/FARFAR (Das & Baker, 2007), 3dRNA (Zhang et al., 2020)) depend on existing structures but are limited by available data. Deep learning models like DeepFoldRNA (Pearce et al., 2022), RhoFold (Shen et al., 2022), RoseTTAFoldNA (Baek et al., 2024), and trRosettaRNA (Wang et al., 2023) show promise in predicting 3D structures from sequence data but face challenges with novel RNA families due to RNA’s conformational flexibility (Kulkarni et al., 2023).

Despite these advances, there is a gap in applying 2D and 3D modeling techniques to RNA property prediction. Most works focus on 1D representations and overlook the potential of geometric information from 2D and 3D structures. This study is the first to systematically explore the benefits and limitations of incorporating explicit structural data in deep learning-based RNA property prediction.

B MODELS OVERVIEW

1. **Transformer1D:** The Transformer1D model is a standard Transformer architecture adopted for RNA sequence processing. It includes an embedding layer to convert input tokens into dense vectors, positional encoding (PE) to retain sequence order and a multi-layer Transformer encoder to capture long-range dependencies within the sequence.

- 918 2. **Transformer1D2D**: An adaptation of Transformer1D that integrates sequence and 2D graph
919 structure information. The model encodes each nucleotide and incorporates BPP features, com-
920 bining standard Transformer with positional encoding and a convolutional layer on the graph
921 adjacency matrix. This convolutional output is added to the attention matrix, enabling the model
922 to capture both sequential and structural dependencies.
- 923 3. **Graph Convolutional Network (GCN)**: A basic model in graph learning that aggregates and
924 processes node features from local neighborhoods to capture both node characteristics and graph
925 structure, making it effective for tasks like node classification.
- 926 4. **Graph Attention Network (GAT)**: Enhances graph convolutions by assigning different impor-
927 tance to neighboring nodes through local attention mechanisms, allowing the model to focus on
928 more relevant nodes during feature aggregation.
- 929 5. **ChebNet**: A spectral GNN that utilizes Chebyshev polynomials to approximate the graph Lapla-
930 cian, enabling graph convolutions with global structural context. This approach allows ChebNet
931 to approximate global graph features with lower computational complexity.
- 932 6. **Graph Transformer**: This model uses Laplacian positional encoding to integrate structural in-
933 formation from the graph’s Laplacian into node features, which are then processed by Trans-
934 former layers. This enables aligning the sequential nature of transformer layers with graph topol-
935 ogy.
- 936 7. **GraphGPS**: A hybrid model combining GNNs with transformers to capture both local and global
937 graph information. It uses GNNs for local feature aggregation and transformers for long-range
938 dependencies, making it effective for complex graph tasks requiring both local and global context.
- 939 8. **SchNet**: An SE(3)-invariant network designed for molecular property prediction on geometric
940 graphs of atomic systems. It operates by modeling interactions through continuous-filter con-
941 volutional layers. Since the continuous-filter in SchNet is conditioned on distance features, it
942 maintains invariance to rotations and translations of atom coordinates.
- 943 9. **E(n)-Equivariant Graph Neural Network (EGNN)**: An equivariant network for geometric
944 graphs with rotations, translations, and reflections symmetry. The EGNN operates by as non-
945 linear message passing between scalar-invariant and vector equivariant quantities.
- 946 10. **FAENet**: FAENet, or Frame Averaging Equivariant Network, is a lightweight and scalable Graph
947 Neural Network designed for materials modeling. It introduces Stochastic Frame Averaging to
948 achieve E(3)-equivariance through data transformations rather than architectural constraints, en-
949 abling superior accuracy and scalability on tasks like molecular and materials property prediction.
- 950 11. **GVPGNN**: Geometric Vector Perceptron GNN is a graph-based model designed to learn from
951 3D molecular structures by integrating geometric and relational information. It uses Geometric
952 Vector Perceptrons to encode scalar and vector features, enabling effective modeling of both
953 protein structure and interactions.
- 954 12. **DimeNet**: Directional Message Passing Neural Network leverages directional message passing
955 to encode both distance and angular information between atoms. It utilizes spherical harmonics
956 and Bessel functions for rotation equivariant message representations, enabling precise modeling
957 of molecular interactions.
- 958 13. **FastEGNN**: FastEGNN introduces virtual nodes to traditional equivariant GNNs, enabling
959 global message passing while maintaining scalability. These virtual nodes are designed to ap-
960 proximate and enhance real node interactions, ensuring E(3)-equivariance for efficient modeling
961 of large geometric graphs.

962 C MEMORY AND COMPUTATIONAL CONSTRAINTS

963
964 In this section, we compare the models based on run times and GPU memory. Both Trans-
965 former1D2D and 3D models (even with nucleotide pooling) encounter out-of-memory (OOM) is-
966 sues when processing longer sequences, such as those in the Fungal dataset (Table 1). This high-
967 lights the need for optimization to handle longer sequences. Figure 7 shows that Transformer1D
968 scales poorly in both runtime and memory due to its expensive attention mechanism, and Trans-
969 former1D2D faces additional challenges by processing the sequence and adjacency matrix simulta-
970 neously. In contrast, simpler 2D models like GCN, GAT, and ChebNet are more efficient. 3D models
971

also scale poorly with sequence length due to the increasing number of atoms. Overall, 2D models provide a good balance between computational demands and performance for encoding structural information.

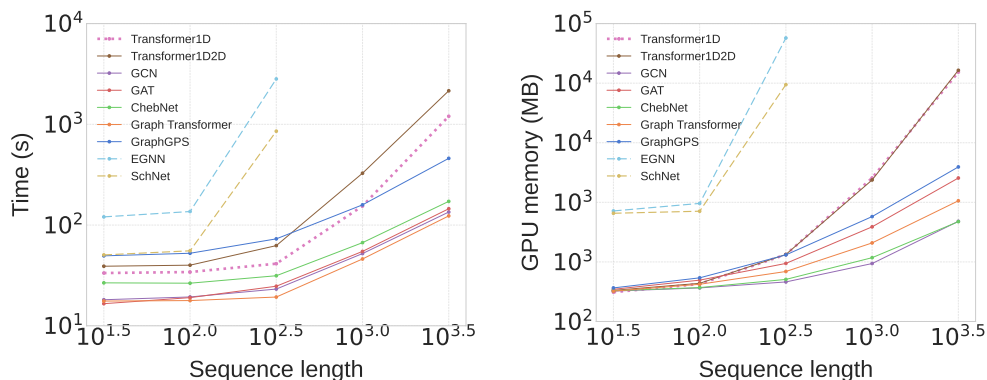


Figure 7: **Running time and memory usage comparison across models.** (1) Running time vs. sequence length (left): Transformer1D and Transformer1D2D scale poorly with sequence length due to expensive attention mechanisms and simultaneous processing of sequences and adjacency matrices, while simpler 2D models like GCN, GAT, and ChebNet are more efficient. (2) Memory usage vs. sequence length (right): Transformer1D2D and 3D models face out-of-memory issues with longer sequences, especially in the largest Fungal dataset, whereas 2D models use memory more efficiently, balancing computational demands and structural encoding.

D DETAILED TASK DESCRIPTIONS

To comprehensively evaluate RNA property prediction models, we define five tasks that simulate real-world experimental challenges. These tasks are designed to assess the performance, efficiency, and robustness of models under various conditions encountered in RNA research and application. Below, we provide detailed explanations for each task, their scientific motivation, and their relevance to practical RNA property prediction.

D.1 TASK 1: IMPACT OF STRUCTURAL INFORMATION ON PREDICTION PERFORMANCE

Motivation: RNA molecules fold into complex secondary (2D) and tertiary (3D) structures that dictate their functional properties. While traditional ML approaches often rely solely on the nucleotide sequence (1D representation), it is well-known in chemistry and biology that structural information influences RNA properties (Schlick & Pyle, 2017). However, the extent to which geometric representations can improve performance of ML models remains unclear.

Task Definition: We evaluate multiple models across three classes (models described in main text):

- **1D models:** Utilize only the linear sequence of nucleotides.
- **2D models:** Incorporate RNA secondary structure, such as base-pairing interactions.
- **3D models:** Leverage full tertiary structural information, including spatial arrangements of nucleotides.

By comparing their performance across diverse datasets, this task quantifies the benefits of using geometric information. Specifically, we aim to determine if models with explicit 2D or 3D inputs outperform sequence-only models, thereby highlighting the added value of structural representations in RNA property prediction.

Significance: This analysis addresses the gap in existing literature, where the impact of structural information on RNA property prediction remains underexplored. The findings inform whether additional computational costs associated with structural modeling are justified by performance gains.

D.2 TASK 2: MODEL EFFICIENCY IN LIMITED TRAINING DATA SETTINGS

Motivation: High-quality RNA datasets with experimentally measured properties are scarce due to the technical difficulty and cost of experimental data acquisition (Byron et al., 2016; Teufel & Sobetzko, 2022). In such scenarios, models must be sample-efficient, learning effectively from small datasets.

Task Definition: Let $D = \{X, Y\}$ represent a dataset, where X is the RNA input and Y is the property label. For this task, we define subsets D_α by sampling a fraction α of the original dataset. We evaluate models trained on varying α values (e.g., $\alpha = 25\%, 50\%, 75\%$) to assess how performance scales with reduced training data.

Significance: This task simulates real-world scenarios where large labeled datasets are unavailable. It evaluates the ability of different models to generalize from limited data, providing insights into their efficiency and practical applicability.

D.3 TASK 3: PERFORMANCE WITH PARTIAL SEQUENCE LABELING

Motivation: In nucleotide-level RNA datasets, labels for molecular properties (e.g., binding affinities or reactivity) are often available only for a subset of nucleotides in a sequence (Wayment-Steele et al., 2022b). This is due to the high cost of annotating every nucleotide experimentally.

Task Definition: We consider datasets where only the first ℓ -nucleotide positions in each sequence are labeled, representing partial sequence labeling. Models are trained using these incomplete labels and evaluated on their ability to predict properties across the full sequence. Performance is assessed using datasets with varying ℓ -label fractions.

Significance: This task reflects a critical real-world challenge where complete annotations are unavailable. It assesses a model’s ability to generalize from partial labels to unseen portions of RNA sequences, a valuable capability for applications with sparse experimental data.

D.4 TASK 4: ROBUSTNESS TO SEQUENCING NOISE

Motivation: RNA sequencing technologies often introduce noise in the form of random nucleotide errors (e.g., insertions, deletions, or substitutions) (Ozsolak & Milos, 2011; Fox et al., 2014). This noise propagates through derived RNA structures (2D and 3D), potentially degrading model performance. Understanding how well models handle noise is crucial for their reliable deployment.

Task Definition: To simulate realistic sequencing errors, we introduce controlled noise levels into RNA sequences during both training and testing. Models are evaluated for their ability to maintain performance under consistent noise conditions, representing a scenario where noise characteristics are stable across experimental phases.

Significance: This task assesses a model’s robustness in practical settings where sequencing noise is unavoidable. It provides insights into the resilience of RNA models to variations in input quality.

D.5 TASK 5: GENERALIZATION TO OUT-OF-DISTRIBUTION (OOD) DATA

Motivation: RNA models are often trained on high-quality experimental datasets but deployed in conditions where data characteristics differ significantly due to variations in sequencing platforms or protocols (Tran et al., 2020; Tom et al., 2017). This mismatch can lead to performance degradation.

Task Definition: We evaluate models trained on clean RNA data and tested on datasets with higher levels of noise (representing OOD conditions). Performance metrics are analyzed as a function of increasing noise, quantifying the models’ ability to generalize to unseen distributions.

Significance: This task mirrors real-world deployment scenarios where models encounter noisy or biased data. It highlights the limitations of models trained on idealized datasets and informs strategies for improving generalization under OOD conditions.

E DISCUSSION ON ADVANCED MODEL ARCHITECTURES

E.1 ENHANCING 3D RNA PREDICTION WITH HIGH-DEGREE STEERABLE FEATURES

Apart from the 3D models considered in this work, models using high-degree steerable features such as TFN (Thomas et al., 2018), MACE (Batatia et al., 2022) and NequIP (Batzner et al., 2022) represent an important aspect of equivariant models, with potential to enhance model expressiveness by incorporating higher-order information. While memory constraints have limited their practical implementation in our current work, techniques such as scalarization of high-degree steerable features, as demonstrated in works such as HEGNN (Frank et al., 2024) and SO3krates (Cen et al., 2024), could address this challenge. For instance, HEGNN can improve the expressivity of equivariant GNNs by mitigating expressivity degeneration on symmetric graphs and leveraging higher-order representations. Although 3D RNA graphs are too complex to be considered symmetric, the ability to handle high-degree steerable features in large RNA graphs, with hundreds of nucleotides and thousands of atoms, remains valuable and has the potential to improve performance. Future work can explore such methods to improve 3D RNA prediction.

E.2 MITIGATING SEQUENCING NOISE

Notably, most studies in this field do not explicitly address sequencing noise common for RNA in model architecture design, prompting a need to explore effective strategies for mitigating its impact. An effective way to handle noise can be through ensemble methods. For instance, combining 1D, 2D, and 3D models by independently learning representations and integrating them via attention mechanisms that dynamically weigh each modality based on task relevance and noise can leverage the robustness of 1D methods while benefiting from the strengths of 2D and 3D approaches and be a good direction for future research.

F ADDITIONAL EXPERIMENTAL INFORMATION

F.1 DATASET STATISTICS

Here, we present the statistics for each dataset used in the paper in Table 2. The datasets are categorized as small, medium, or large based on the number of sequences and sequence length. “Target” refers to the task the dataset is designed to predict, and “# Avg. Atoms” indicates the average number of atoms used in 3D models.

Table 2: The statistics of Tc-Riboswitches, Ribonanza, COVID, and Fungal datasets.

	Tc-Riboswitches	Ribonanza	COVID	Fungal
Dataset Size	Small	Medium	Medium	Large
Task Level	RNA-level	Nucleotide-level	Nucleotide-level	RNA-level
Target	Switching Factor	Degradation	Degradation	Expression
# Sequences	355	2260	4082	7089
Sequence Length	66 - 75	177	107 - 130	150 - 3063
# Labels	1	2	3	1
# Avg. Atoms (for 3D models)	1531	3791	2598	N/A

F.2 COMPARISON OF PARTIAL TRAINING DATA AND PARTIAL SEQUENCE LABELING

To clarify the differences and provide a more detailed explanation, we illustrate two experiments: partial training data and partial sequence labeling (Figure 8).

F.3 DETAILS OF NOISY EXPERIMENTS: ROBUSTNESS AND GENERALIZATION

To create the noisy datasets, we vary the noise ratio r across the values $\{0.05, 0.1, 0.15, 0.2, 0.25, 0.3\}$. For each given noise ratio, we independently mutate the nucleotide at each position in a

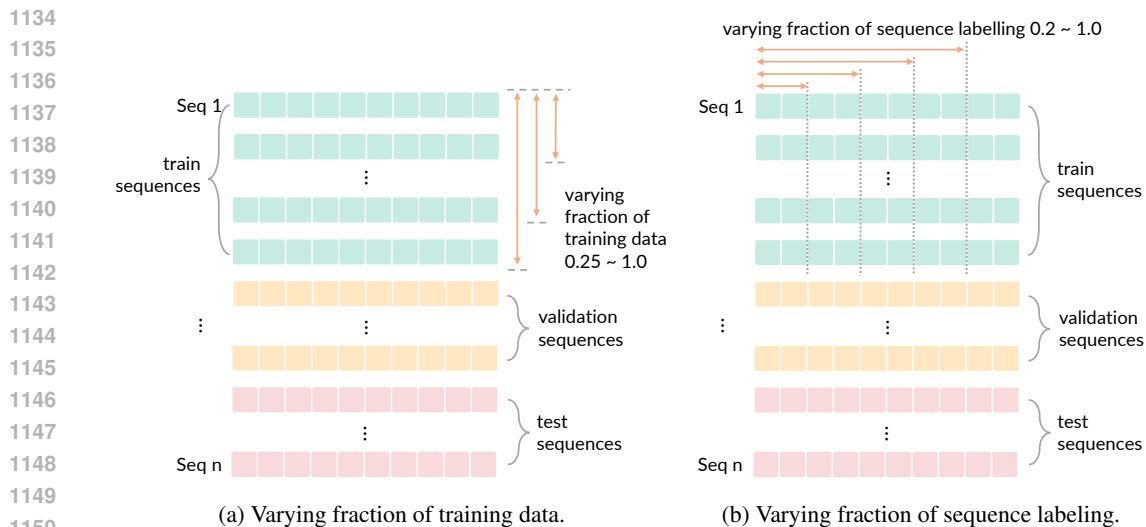


Figure 8: **Comparison of partial training data and partial sequence labeling.** The orange arrows indicate the varying components. (a) utilizes full nucleotide labels but trains on varying fractions of RNA sequences (0.25, 0.5, 0.75, 1.0). (b) uses all training sequences but with varying fractions of nucleotide labels (0.2, 0.4, 0.6, 0.8, 1.0). Therefore, (b) is only for nucleotide-level tasks.

sequence with probability r , as illustrated in Figure 9. The resulting mutated sequence is then passed to the 2D and 3D prediction tools to generate the corresponding structures. Figure 4 gives a comprehensive illustration of getting noisy 1D, 2D, and 3D structures.

For the robustness experiments, all training, validation, and testing are conducted on the noisy datasets. In contrast, for the generalization experiments, the model is trained and validated on clean datasets, and its performance is tested on noisy datasets with varying noise ratios.

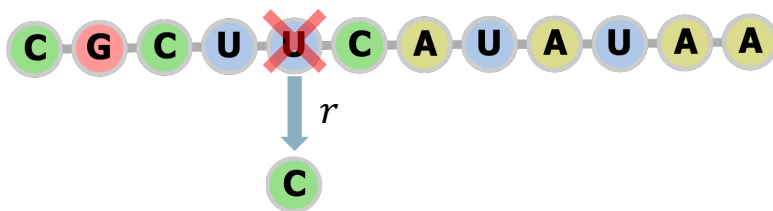


Figure 9: Mutation the nucleotide at each position independently with the probability r .

F.4 ANALYSIS OF TRANSFORMER1D AND TRANSFORMER1D2D

To further validate that incorporating structural information contributes to the final results, we analyze the attention maps generated by Transformer1D and Transformer1D2D. Fig. 10 illustrates the average attention maps across all heads before the final output layer for both the models for a randomly selected RNA sequence. The attention maps of Transformer1D2D exhibit a striking similarity to both the adjacency matrix and the BPP matrix, whereas the attention maps from the standard Transformer model seem to suggest that the model does not learn to attend to the structural features. Moreover, we quantify this observation by computing the cosine similarity between the attention maps of the models and the true adjacency matrix and BPP for all sequences in the COVID dataset. The results, reported in Table 3 show that Transformer1D2D achieves much higher similarity scores compared to the 1D Transformer alone. This reinforces the conclusion that explicit encoding of structural information is essential for improved model performance.

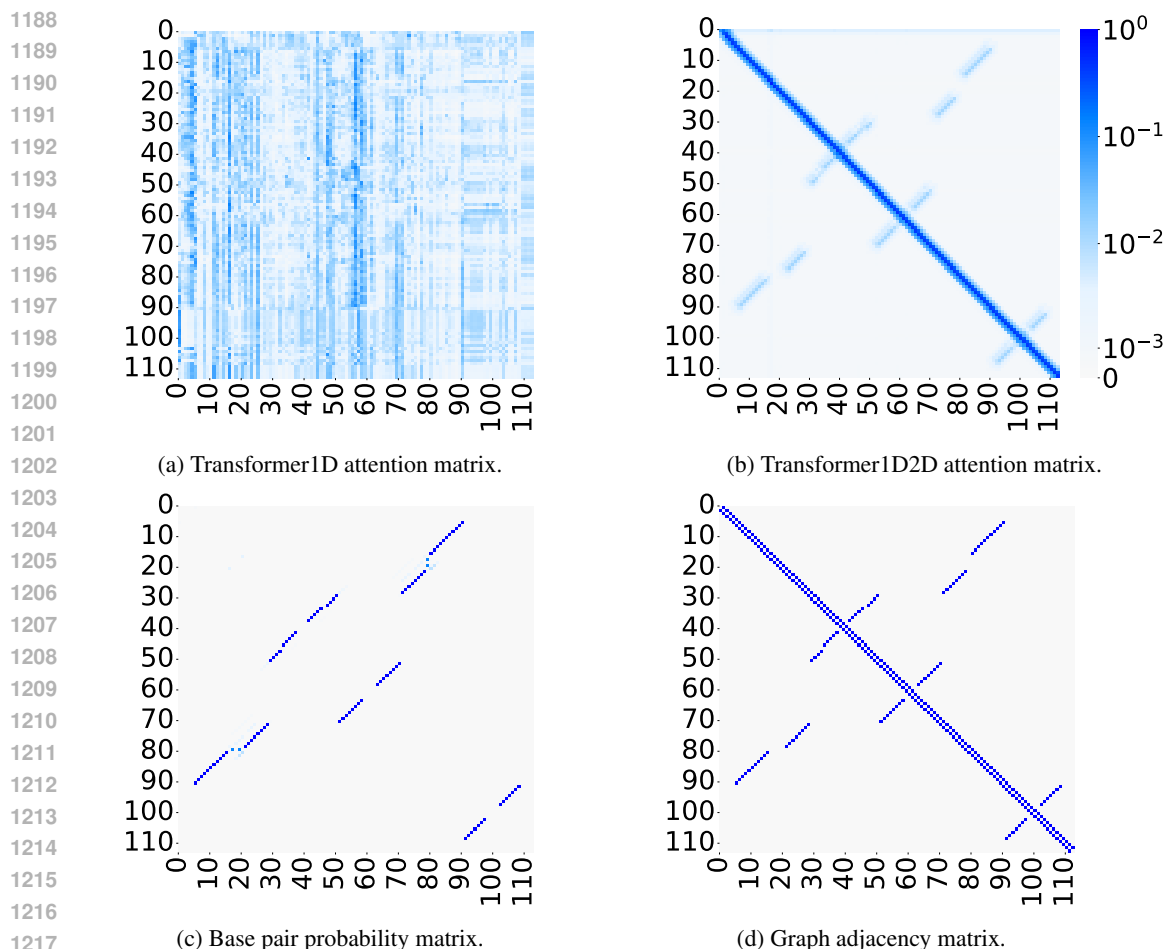


Figure 10: **The heatmaps of matrices in Transformer1D and Transformer1D2D.** Attention maps from Transformer1D2D exhibit a striking resemblance to both the adjacency matrix and BPP matrix, highlighting the model’s ability to learn structural features. In contrast, the standard Transformer struggles with this task, as shown by lower cosine similarity scores, reinforcing the conclusion that explicitly encoding structural information is crucial for enhanced model performance.

Table 3: **Cosine similarity values for different models.** Cosine similarity scores between the attention maps and the true adjacency and BPP matrices for all sequences in the COVID dataset demonstrate that Transformer1D2D significantly outperforms the standard Transformer. These results underscore the importance of explicitly encoding structural information for superior model performance.

Model	Cosine similarity adjacency	Cosine similarity BPP
Transformer1D	0.107	0.090
Transformer1D2D	0.448	0.672

G ANALYSIS OF NOISE IN 3D STRUCTURES

As mentioned in the main context, predicted 3D structures consistently exhibit noise. In this section, we analyze this issue from two perspectives: sensitivity to sequence length and variability across different prediction tools.

G.1 IMPACT OF SEQUENCE LENGTH ON 3D STRUCTURE PREDICTION NOISE

To investigate the hypothesis that longer sequences result in greater noise in 3D structure predictions, we randomly selected a COVID and Tc-Riboswitches dataset sequence and generated structures using four state-of-the-art 3D structure prediction tools: RhoFold (Shen et al., 2022), RNAComposer (Xu et al., 2014), trRosetta (Baek et al., 2024), and SimRNA (Boniecki et al., 2016). High variability among these predicted structures would indicate significant uncertainty in absolute atom positions. We quantified this noise by aligning the structures using the Kabsch algorithm (Kabsch, 1976) and computing the pairwise RMSD values, resulting in a 4x4 matrix showing structural deviations between each pair of tools (see Table 4). The observed pairwise RMSD values ranged from 16 to 45 Å for the COVID dataset and from 11 to 15 Å for the Tc-Riboswitches dataset, reflecting substantial variability and suggesting considerable noise in the 3D predictions. This level of structural inaccuracy likely contributes to the poorer performance of 3D models. However, we found that 3D models outperform 1D models for shorter sequences, such as those in the Tc-Riboswitches dataset (67 to 73 nucleotides long). This improved performance is due to the lower noise in 3D predictions for shorter sequences, a phenomenon supported by previous studies (Nithin et al., 2024; Ponce-Salvatierra et al., 2019) and also exhibited by the comparatively smaller RMSD values reported in Table 4 for Tc-Riboswitches dataset. The reduced complexity of shorter sequences allows 3D models to capture structural details more accurately, thereby enhancing performance and validating that accurate 3D structure encoding can outperform 1D models.

Table 4: **Pairwise RMSD values (in Å) between 3D structure prediction tools for the COVID dataset (left) and Tc-Riboswitches dataset (right).** The results indicate larger noise in predictions for longer COVID sequences.

COVID	RhoFold	trRosetta	SimRNA	Composer
RhoFold	0	39.05192	44.76146	45.45994
trRosetta	39.05192	0	22.54974	18.17359
SimRNA	44.76146	22.54974	0	16.73399
Composer	45.45994	18.17359	16.73399	0
Tc-Ribo	RhoFold	trRosetta	SimRNA	Composer
RhoFold	0	14.338	11.996	15.056
trRosetta	14.338	0	12.932	14.916
SimRNA	11.996	12.932	0	14.243
Composer	15.056	14.916	14.243	0

G.2 IMPACT OF DIFFERENT 3D PREDICTION TOOLS

In this section, we demonstrate the significant differences in 3D structures predicted by various tools. We compare the 3D structure obtained from RhoFold (Shen et al., 2022), which serves as our default method, with those predicted by RNAComposer (Xu et al., 2014), trRosetta (Baek et al., 2024), and SimRNA (Boniecki et al., 2016). Each structure is visualized side by side with RhoFold in Figure 11 to facilitate a more intuitive comparison. As observed, these structures predicted by each tool vary considerably.

H REPRODUCTION

This section outlines the necessary details to reproduce all experiments discussed in this paper. The code will be made publicly available upon acceptance.

H.1 TRAINING DETAILS

All experiments were conducted on a single NVIDIA A100 GPU. For each baseline, hyperparameters were optimized using Optuna (Akiba et al., 2019), restricting the search to models with fewer

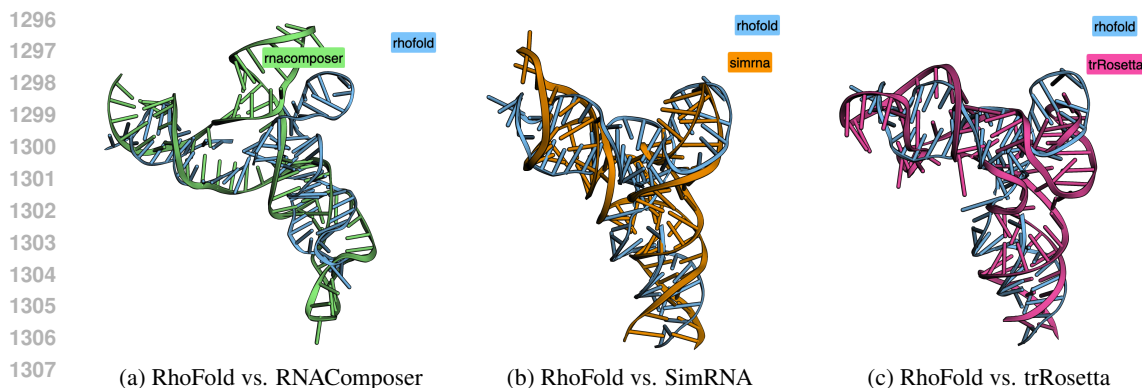


Figure 11: Comparison of RhoFold against other 3D structure prediction tools on an example sequence from Tc-Riboswitches dataset.

than 10 million parameters that fit within the memory constraints of an 80GB NVIDIA A100 GPU. Most baseline implementations were sourced from PyTorch Geometric (Fey & Lenssen, 2019). The Transformer1D model was adapted to Transformer1D2D as detailed in the paper. For EGNN, we utilized the authors’ implementation (Satorras et al., 2021), and for SchNet, the implementation from (Joshi et al., 2023) was used.

H.2 HYPERPARAMETERS

This section provides a comprehensive overview of the hyperparameters used in each baseline model, facilitating reproducibility and understanding of the model configurations.

Common hyperparameters across these models include `in_channels`, which specifies the number of input features, `hidden`, which determines the number of hidden units in each hidden layer, and `out_channels`, which defines the number of output features. The `L` parameter controls the number of layers in the network, and the `dropout` parameter sets the dropout rate for regularization. The `lr` parameter specifies the learning rate, and `weight_decay` sets the weight decay for regularization of the optimizer. For graph-level tasks, the `pool` parameter specifies the pooling method, which can be `mean`, `max`, or `add`.

Transformer1D is a standard Transformer architecture for RNA sequence processing. It includes an embedding layer to convert input tokens into dense vectors, positional encoding (PE) to retain sequence order and a multi-layer Transformer encoder to capture complex dependencies within the sequence. There are some hyperparameters from the original transformer (Vaswani et al., 2017). `nhead`, which defines the number of attention heads in each Transformer layer; `num_encoder_layers`, which controls the number of encoder layers in the Transformer; `d_model`, which determines the dimensionality of the embeddings and the model; `dim_feedforward`, which sets the dimensionality of the feedforward network model. To shrink the search space, we set `d_model` and `dim_feedforward` as the same with a new hyperparameter `hidden`.

Transformer1D2D is an adaptation of Transformer1D that integrates both sequence and 2D graph structure information. In addition to encoding each nucleotide, the model incorporates base pair probabilities (BPP) features for each nucleotide. It combines a standard Transformer with positional encoding and a convolutional layer applied to the graph adjacency matrix. This convolutional output is added to the Transformer’s attention matrix, allowing the model to incorporate graph structure into its attention mechanism. This design captures both the sequential and structural dependencies in RNA data, improving predictive performance. The unique hyperparameter for this model is `kernel_size`, which specifies the size of the convolutional kernel.

GAT includes the unique hyperparameters `gat_heads`, which specify the number of attention heads in each GAT layer.

1350 **ChebNet** model has the unique hyperparameter `power`, which specifies the polynomial order for
1351 the Chebyshev convolution.

1352 **GraphGPS** and **Graph Transformer** includes `heads`, which specifies the number of attention
1353 heads in each layer, and `pe_dim`, which defines the dimensionality of positional encoding.
1354

1355 **EGNN** and **SchNet** are 3D models that operate at two granularities within the network: atom
1356 layers and nucleotide layers. The two types of layers are connected through nucleotide pooling.
1357 Atom layers use atoms as nodes, while nucleotide layers use nucleotides as nodes. Both the atom
1358 layer and nucleotide layer employ a point cloud setting and calculate edges based on the distance
1359 between two nodes. An edge is considered to exist if the distance is smaller than a certain threshold.
1360 Therefore, EGNN and SchNet share the following hyperparameters: `L_atom`, which denotes the
1361 number of atom layers; `L_nt`, which specifies the number of nucleotide layers; `threshold_atom`,
1362 which is the threshold for edges in atom layers; and `threshold_nt`, which is the threshold for
1363 edges in nucleotide layers.

1364 For SchNet, the unique hyperparameters include `num_filters`, which refers to the number of
1365 filters used in convolutional layers, and `num_gaussians`, which indicates the number of Gaussian
1366 functions used for radial filters. For a more detailed explanation of these hyperparameters, please
1367 refer to (Schütt et al., 2017).

1368 To ensure a fair comparison, the best hyperparameter configuration for each method was selected
1369 based on validation set performance. We report the mean performance and standard deviation across
1370 5 random splits on the test set. For the COVID and Ribonanza datasets, we performed hyperparam-
1371 eter searching only on the COVID dataset and applied the same configuration to Ribonanza, as the
1372 two datasets share similar properties. The optimal hyperparameters are shown in Table 5.

1372 I ADDITIONAL RESULTS

1373 In this section, we present the additional results supporting Figures 2, 3, 5, and 6 in main text.

1375 I.1 IMPACT OF DATA AVAILABILITY

1376 The detailed results of partial training data from Figure 2 are shown in Tables 6, 7, and 8.
1377

1378 I.2 IMPACT OF PARTIAL LABELING

1379 The detailed results of the partial labeling sequence from Figure 3 are shown in Tables 9 and 10.
1380

1381 I.3 ROBUSTNESS TO SEQUENCING NOISE

1382 The results of the robustness experiment from Figure 5 are shown in Tables 11, 12, 13, and 14.
1383

1384 I.4 GENERALIZATION TO OOD DATA

1385 The results of the generalization experiment from Figure 6 are shown in Tables 15, 16, 17, and 18.
1386
1387
1388
1389
1390
1391
1392
1393
1394
1395
1396
1397
1398
1399
1400
1401
1402
1403

	Hyperparameter	COVID & Ribonanza	Tc-riboswitches	Fungal
1404				
1405				
1406	Transformer1D	lr	0.001	0.0005
1407		weight_decay	0	0.0005
1408		hidden	128	64
1409		nhead	8	8
1410		num_encoder_layers	8	6
1411		pool	/	mean
1412	Transformer1D2D	lr	0.001	0.005
1413		weight_decay	0	0
1414		hidden	256	32
1415		nhead	16	4
1416		num_encoder_layers	8	4
1417		pool	mean	mean
1418	GCN	kernel_size	5	5
1419		lr	0.001	0.0001
1420		weight_decay	0	0
1421		hidden	1024	512
1422		L	7	5
1423		dropout	0.3	0.1
1424		pool	/	max
1425	ChebNet	lr	0.001	0.005
1426		weight_decay	0	0.0005
1427		hidden	512	256
1428		L	5	7
1429		dropout	0.3	0.3
1430		power	6	2
1431		pool	/	max
1432	GAT	lr	0.001	0.005
1433		weight_decay	0	0
1434		hidden	256	1024
1435		L	7	3
1436		dropout	0.1	0.1
1437		heads	4	2
1438		pool	/	add
1439	Graph Transformer	lr	0.001	0.005
1440		weight_decay	0	0
1441		hidden	128	64
1442		L	7	5
1443		heads	4	1
1444		pool	/	add
1445	GraphGPS	lr	0.001	1e-5
1446		weight_decay	0	0.0005
1447		hidden	256	256
1448		L	5	7
1449		heads	2	1
1450		pool	/	add
1451	EGNN	lr	0.0005	0.001
1452		weight_decay	0	0
1453		hidden	256	256
1454		L_atom	3	3
1455		L_nt	2	1
1456		threshold_atom	1.6	1.6
1457		threshold_nt	22	22
1458	SchNet	lr	0.0005	0.001
1459		weight_decay	0	0
1460		hidden	128	128
1461		L_atom	1	1
1462		L_nt	2	4
1463		threshold_atom	1.6	1.8
1464		threshold_nt	44	88
1465	num_filters	128	256	
1466		num_gaussians	50	50

Table 5: Best hyperparameters for each model and dataset. Hyperparameters are searched by Optuna. COVID and Ribonanza share the same hyperparameters.

Table 6: Performance (MCRMSE) of different models across various training data (mean \pm standard deviation) fractions on COVID dataset.

COVID	0.25	0.50	0.75	1.00
Transformer1D	0.429 \pm 0.018	0.410 \pm 0.016	0.375 \pm 0.018	0.361 \pm 0.017
Transformer1D2D	0.345 \pm 0.010	0.330 \pm 0.011	0.306 \pm 0.014	0.305 \pm 0.012
GCN	0.389 \pm 0.008	0.377 \pm 0.009	0.358 \pm 0.014	0.359 \pm 0.009
GAT	0.352 \pm 0.011	0.342 \pm 0.009	0.320 \pm 0.014	0.315 \pm 0.006
ChebNet	0.320 \pm 0.011	0.309 \pm 0.009	0.286 \pm 0.018	0.279 \pm 0.007
Graph Transformer	0.356 \pm 0.008	0.344 \pm 0.007	0.324 \pm 0.016	0.318 \pm 0.008
GraphGPS	0.367 \pm 0.018	0.362 \pm 0.005	0.344 \pm 0.010	0.332 \pm 0.013
EGNN	0.398 \pm 0.001	0.391 \pm 0.013	0.368 \pm 0.013	0.364 \pm 0.003
SchNet	0.419 \pm 0.003	0.414 \pm 0.011	0.392 \pm 0.011	0.390 \pm 0.006
FastEGNN	0.460 \pm 0.018	0.452 \pm 0.015	0.443 \pm 0.016	0.444 \pm 0.003

Table 7: Performance (MCRMSE) of different models across various fractions of training data (mean \pm standard deviation) on Ribonanza dataset.

Ribonanza	0.25	0.50	0.75	1.00
Transformer1D	0.777 \pm 0.014	0.740 \pm 0.005	0.739 \pm 0.001	0.705 \pm 0.015
Transformer1D2D	0.630 \pm 0.016	0.553 \pm 0.015	0.541 \pm 0.018	0.514 \pm 0.004
GCN	0.668 \pm 0.018	0.618 \pm 0.017	0.612 \pm 0.013	0.595 \pm 0.006
GAT	0.600 \pm 0.018	0.553 \pm 0.026	0.544 \pm 0.012	0.534 \pm 0.006
ChebNet	0.537 \pm 0.019	0.494 \pm 0.022	0.499 \pm 0.007	0.468 \pm 0.002
Graph Transformer	0.567 \pm 0.019	0.529 \pm 0.013	0.529 \pm 0.010	0.515 \pm 0.001
GraphGPS	0.581 \pm 0.021	0.529 \pm 0.015	0.540 \pm 0.004	0.523 \pm 0.003
EGNN	0.694 \pm 0.010	0.650 \pm 0.010	0.632 \pm 0.015	0.619 \pm 0.007
SchNet	0.768 \pm 0.008	0.724 \pm 0.013	0.715 \pm 0.015	0.685 \pm 0.006
FastEGNN	0.795 \pm 0.007	0.788 \pm 0.002	0.774 \pm 0.016	0.753 \pm 0.015

Table 8: Performance (MCRMSE) of different models across various fractions of training data (mean \pm standard deviation) on Fungal dataset.

Fungal	0.25	0.50	0.75	1.00
Transformer1D	1.510 \pm 0.006	1.446 \pm 0.014	1.475 \pm 0.035	1.417 \pm 0.005
GCN	1.243 \pm 0.064	1.244 \pm 0.128	1.151 \pm 0.077	1.192 \pm 0.077
GAT	1.211 \pm 0.125	1.168 \pm 0.033	1.146 \pm 0.109	1.112 \pm 0.035
ChebNet	1.125 \pm 0.097	1.011 \pm 0.010	1.008 \pm 0.009	0.973 \pm 0.003
Graph Transformer	1.415 \pm 0.014	1.331 \pm 0.163	1.306 \pm 0.127	1.317 \pm 0.002
GraphGPS	1.289 \pm 0.071	1.377 \pm 0.127	1.357 \pm 0.106	1.025 \pm 0.081

Table 9: Performance (MCRMSE) of different models across various fractions of sequence labeling (mean \pm standard deviation) on COVID dataset.

COVID	0.2	0.4	0.6	0.8	1.0
Transformer1D	0.654 \pm 0.040	0.559 \pm 0.011	0.480 \pm 0.004	0.429 \pm 0.034	0.361 \pm 0.017
Transformer1D2D	0.502 \pm 0.002	0.470 \pm 0.052	0.374 \pm 0.007	0.325 \pm 0.006	0.305 \pm 0.012
GCN	0.450 \pm 0.012	0.416 \pm 0.012	0.397 \pm 0.012	0.378 \pm 0.011	0.359 \pm 0.009
GAT	0.411 \pm 0.010	0.376 \pm 0.012	0.360 \pm 0.012	0.336 \pm 0.009	0.315 \pm 0.006
ChebNet	0.380 \pm 0.007	0.344 \pm 0.008	0.325 \pm 0.009	0.299 \pm 0.007	0.279 \pm 0.007
Graph Transformer	0.415 \pm 0.012	0.379 \pm 0.011	0.362 \pm 0.011	0.338 \pm 0.004	0.318 \pm 0.008
GraphGPS	0.428 \pm 0.015	0.400 \pm 0.017	0.376 \pm 0.013	0.351 \pm 0.007	0.332 \pm 0.013
EGNN	0.436 \pm 0.014	0.421 \pm 0.010	0.407 \pm 0.004	0.385 \pm 0.006	0.364 \pm 0.003
SchNet	0.442 \pm 0.004	0.429 \pm 0.005	0.413 \pm 0.001	0.407 \pm 0.005	0.390 \pm 0.006
FastEGNN	0.497 \pm 0.004	0.490 \pm 0.007	0.466 \pm 0.007	0.469 \pm 0.009	0.444 \pm 0.003

Table 10: Performance (MCRMSE) of different models across various fractions of sequence labeling (mean \pm standard deviation) on Ribonanza dataset.

Ribonanza	0.2	0.4	0.6	0.8	1.0
Transformer1D	1.137 \pm 0.163	0.929 \pm 0.023	0.823 \pm 0.018	0.742 \pm 0.013	0.705 \pm 0.015
Transformer1D2D	0.859 \pm 0.025	0.638 \pm 0.013	0.632 \pm 0.028	0.568 \pm 0.013	0.514 \pm 0.004
GCN	1.191 \pm 0.031	1.026 \pm 0.079	1.111 \pm 0.206	1.070 \pm 0.137	0.595 \pm 0.006
GAT	0.703 \pm 0.015	0.632 \pm 0.025	0.612 \pm 0.030	0.560 \pm 0.010	0.534 \pm 0.006
ChebNet	0.614 \pm 0.013	0.546 \pm 0.008	0.540 \pm 0.008	0.514 \pm 0.006	0.468 \pm 0.002
Graph Transformer	0.719 \pm 0.043	0.607 \pm 0.020	0.584 \pm 0.015	0.552 \pm 0.013	0.515 \pm 0.001
GraphGPS	0.743 \pm 0.058	0.663 \pm 0.026	0.627 \pm 0.024	0.651 \pm 0.026	0.523 \pm 0.003
EGNN	0.882 \pm 0.010	0.722 \pm 0.021	0.687 \pm 0.008	0.665 \pm 0.013	0.619 \pm 0.007
SchNet	0.810 \pm 0.002	0.781 \pm 0.009	0.750 \pm 0.009	0.725 \pm 0.004	0.685 \pm 0.006
FastEGNN	1.223 \pm 0.008	0.929 \pm 0.008	0.860 \pm 0.004	0.837 \pm 0.004	0.753 \pm 0.015

Table 11: Performance (MCRMSE) of various models in **robustness** experiments on the **COVID** dataset (mean \pm standard deviation).

Model	0.00	0.05	0.10	0.15	0.20	0.25	0.30
Transformer1D	0.361 \pm 0.017	0.386 \pm 0.015	0.400 \pm 0.010	0.409 \pm 0.006	0.428 \pm 0.005	0.435 \pm 0.003	0.449 \pm 0.011
Transformer1D2D	0.305 \pm 0.012	0.373 \pm 0.007	0.403 \pm 0.007	0.428 \pm 0.011	0.444 \pm 0.015	0.457 \pm 0.009	0.463 \pm 0.009
GCN	0.359 \pm 0.009	0.436 \pm 0.009	0.464 \pm 0.011	0.481 \pm 0.010	0.491 \pm 0.012	0.497 \pm 0.009	0.501 \pm 0.009
GAT	0.315 \pm 0.006	0.409 \pm 0.009	0.448 \pm 0.011	0.471 \pm 0.010	0.484 \pm 0.012	0.494 \pm 0.011	0.500 \pm 0.010
ChebNet	0.279 \pm 0.007	0.368 \pm 0.003	0.423 \pm 0.009	0.456 \pm 0.007	0.471 \pm 0.009	0.481 \pm 0.010	0.487 \pm 0.008
Graph Transformer	0.318 \pm 0.008	0.403 \pm 0.008	0.441 \pm 0.012	0.467 \pm 0.011	0.480 \pm 0.012	0.487 \pm 0.010	0.494 \pm 0.011
GraphGPS	0.332 \pm 0.013	0.408 \pm 0.012	0.441 \pm 0.010	0.464 \pm 0.014	0.475 \pm 0.012	0.484 \pm 0.012	0.487 \pm 0.008
EGNN	0.364 \pm 0.003	0.432 \pm 0.012	0.467 \pm 0.009	0.486 \pm 0.009	0.499 \pm 0.011	0.505 \pm 0.012	0.511 \pm 0.011
SchNet	0.390 \pm 0.006	0.447 \pm 0.012	0.477 \pm 0.011	0.496 \pm 0.009	0.507 \pm 0.014	0.513 \pm 0.012	0.517 \pm 0.010
FastEGNN	0.444 \pm 0.003	0.49283 \pm 0.008	0.516 \pm 0.005	0.516 \pm 0.004	0.522 \pm 0.002	0.527 \pm 0.003	0.540 \pm 0.004

Table 12: Performance (MCRMSE) of various models in **robustness** experiments on the **Ribonanza** dataset (mean \pm standard deviation).

Model	0.00	0.05	0.10	0.15	0.20	0.25	0.30
Transformer1D	0.705 \pm 0.015	0.733 \pm 0.010	0.769 \pm 0.014	0.782 \pm 0.005	0.794 \pm 0.010	0.805 \pm 0.017	0.823 \pm 0.005
Transformer1D2D	0.514 \pm 0.004	0.635 \pm 0.004	0.714 \pm 0.014	0.763 \pm 0.008	0.790 \pm 0.009	0.811 \pm 0.014	0.830 \pm 0.008
GCN	0.595 \pm 0.006	0.750 \pm 0.014	0.846 \pm 0.008	0.893 \pm 0.003	0.912 \pm 0.005	0.924 \pm 0.005	0.929 \pm 0.005
GAT	0.534 \pm 0.006	0.691 \pm 0.015	0.785 \pm 0.006	0.850 \pm 0.003	0.877 \pm 0.001	0.904 \pm 0.007	0.915 \pm 0.007
ChebNet	0.468 \pm 0.002	0.611 \pm 0.012	0.720 \pm 0.006	0.802 \pm 0.011	0.841 \pm 0.003	0.876 \pm 0.007	0.897 \pm 0.008
Graph Transformer	0.515 \pm 0.001	0.670 \pm 0.011	0.768 \pm 0.011	0.833 \pm 0.008	0.870 \pm 0.006	0.893 \pm 0.010	0.908 \pm 0.007
GraphGPS	0.523 \pm 0.003	0.677 \pm 0.017	0.772 \pm 0.006	0.832 \pm 0.006	0.872 \pm 0.004	0.896 \pm 0.011	0.912 \pm 0.006
EGNN	0.619 \pm 0.007	0.764 \pm 0.003	0.847 \pm 0.003	0.889 \pm 0.005	0.904 \pm 0.003	0.917 \pm 0.000	0.922 \pm 0.002
SchNet	0.685 \pm 0.006	0.814 \pm 0.006	0.873 \pm 0.004	0.897 \pm 0.004	0.908 \pm 0.004	0.918 \pm 0.005	0.922 \pm 0.005
FastEGNN	0.753 \pm 0.015	0.857 \pm 0.001	0.884 \pm 0.005	0.908 \pm 0.001	0.914 \pm 0.004	0.920 \pm 0.003	0.922 \pm 0.003

Table 13: Performance (MCRMSE) of various models in **robustness** experiments on the **Fungal** dataset (mean \pm standard deviation).

Model	0.00	0.05	0.10	0.15	0.20	0.25	0.30
Transformer1D	1.417 \pm 0.005	1.545 \pm 0.045	1.546 \pm 0.044	1.546 \pm 0.046	1.543 \pm 0.048	1.543 \pm 0.051	1.550 \pm 0.041
GCN	1.192 \pm 0.077	1.222 \pm 0.044	1.255 \pm 0.002	1.277 \pm 0.014	1.269 \pm 0.011	1.328 \pm 0.026	1.294 \pm 0.025
GAT	1.112 \pm 0.035	1.244 \pm 0.074	1.391 \pm 0.155	1.334 \pm 0.099	1.468 \pm 0.056	1.444 \pm 0.094	1.446 \pm 0.092
ChebNet	0.978 \pm 0.000	1.031 \pm 0.003	1.091 \pm 0.007	1.108 \pm 0.009	1.243 \pm 0.005	1.210 \pm 0.014	1.269 \pm 0.007
Graph Transformer	1.342 \pm 0.087	1.267 \pm 0.116	1.409 \pm 0.046	1.426 \pm 0.051	1.442 \pm 0.038	1.413 \pm 0.020	1.450 \pm 0.018
GraphGPS	1.083 \pm 0.131	1.048 \pm 0.095	1.133 \pm 0.057	1.109 \pm 0.040	1.173 \pm 0.071	1.256 \pm 0.016	1.328 \pm 0.041

Table 14: Performance (MCRMSE) of various models in **robustness** experiments on the **Tc-riboswitches** dataset (mean \pm standard deviation).

Model	0.00	0.05	0.10	0.15	0.20	0.25	0.30
Transformer1D	0.705 \pm 0.079	0.698 \pm 0.071	0.736 \pm 0.004	0.672 \pm 0.003	0.739 \pm 0.008	0.694 \pm 0.011	0.675 \pm 0.047
Transformer1D2D	0.633 \pm 0.001	0.697 \pm 0.031	0.742 \pm 0.003	0.708 \pm 0.008	0.681 \pm 0.001	0.762 \pm 0.022	0.738 \pm 0.016
GCN	0.701 \pm 0.004	0.758 \pm 0.003	0.747 \pm 0.005	0.744 \pm 0.004	0.733 \pm 0.013	0.740 \pm 0.011	0.765 \pm 0.009
GAT	0.685 \pm 0.024	0.749 \pm 0.017	0.770 \pm 0.047	0.734 \pm 0.021	0.737 \pm 0.009	0.753 \pm 0.001	0.747 \pm 0.011
ChebNet	0.621 \pm 0.022	0.766 \pm 0.014	0.754 \pm 0.021	0.738 \pm 0.014	0.763 \pm 0.039	0.778 \pm 0.048	0.739 \pm 0.004
Graph Transformer	0.703 \pm 0.054	0.754 \pm 0.005	0.754 \pm 0.006	0.773 \pm 0.008	0.810 \pm 0.087	0.742 \pm 0.004	0.754 \pm 0.005
GraphGPS	0.702 \pm 0.028	0.785 \pm 0.053	0.805 \pm 0.092	0.750 \pm 0.006	0.755 \pm 0.060	0.769 \pm 0.031	1.078 \pm 0.469
EGNN	0.663 \pm 0.010	0.750 \pm 0.001	0.739 \pm 0.002	0.749 \pm 0.005	0.749 \pm 0.001	0.749 \pm 0.001	0.756 \pm 0.013
SchNet	0.655 \pm 0.038	0.762 \pm 0.005	0.742 \pm 0.002	0.771 \pm 0.037	0.746 \pm 0.005	0.791 \pm 0.016	0.730 \pm 0.016
FastEGNN	0.710 \pm 0.010	0.733 \pm 0.007	0.749 \pm 0.006	0.748 \pm 0.006	0.752 \pm 0.008	0.758 \pm 0.017	0.761 \pm 0.010

Table 15: Performance (MCRMSE) of various models in **generalization** experiments on the **COVID** dataset (mean \pm standard deviation).

Model	0.00	0.05	0.10	0.15	0.20	0.25	0.30
Transformer1D	0.361 \pm 0.017	0.382 \pm 0.022	0.402 \pm 0.018	0.436 \pm 0.015	0.461 \pm 0.021	0.478 \pm 0.015	0.494 \pm 0.016
Transformer1D2D	0.305 \pm 0.012	0.406 \pm 0.016	0.466 \pm 0.017	0.513 \pm 0.016	0.545 \pm 0.027	0.581 \pm 0.025	0.596 \pm 0.018
GCN	0.359 \pm 0.009	0.459 \pm 0.011	0.508 \pm 0.011	0.550 \pm 0.014	0.572 \pm 0.016	0.601 \pm 0.014	0.612 \pm 0.008
GAT	0.315 \pm 0.006	0.437 \pm 0.013	0.490 \pm 0.013	0.528 \pm 0.008	0.555 \pm 0.013	0.580 \pm 0.015	0.592 \pm 0.012
ChebNet	0.279 \pm 0.007	0.415 \pm 0.017	0.483 \pm 0.023	0.538 \pm 0.025	0.571 \pm 0.029	0.604 \pm 0.030	0.621 \pm 0.028
Graph Transformer	0.318 \pm 0.008	0.449 \pm 0.015	0.501 \pm 0.018	0.543 \pm 0.015	0.571 \pm 0.019	0.596 \pm 0.014	0.609 \pm 0.014
GraphGPS	0.332 \pm 0.013	0.443 \pm 0.011	0.496 \pm 0.006	0.536 \pm 0.005	0.559 \pm 0.010	0.586 \pm 0.007	0.593 \pm 0.005
EGNN	0.365 \pm 0.011	0.458 \pm 0.014	0.504 \pm 0.018	0.530 \pm 0.020	0.549 \pm 0.021	0.565 \pm 0.022	0.572 \pm 0.022
SchNet	0.390 \pm 0.006	0.457 \pm 0.011	0.491 \pm 0.008	0.515 \pm 0.007	0.531 \pm 0.010	0.543 \pm 0.009	0.556 \pm 0.002
FastEGNN	0.444 \pm 0.003	0.491 \pm 0.020	0.511 \pm 0.014	0.524 \pm 0.009	0.533 \pm 0.006	0.541 \pm 0.003	0.543 \pm 0.001

Table 16: Performance (MCRMSE) of various models in **generalization** experiments on the **Ribonanza** dataset (mean \pm standard deviation).

Model	0.00	0.05	0.10	0.15	0.20	0.25	0.30
Transformer1D	0.705 \pm 0.015	0.747 \pm 0.005	0.796 \pm 0.006	0.828 \pm 0.008	0.860 \pm 0.013	0.886 \pm 0.013	0.899 \pm 0.003
Transformer1D2D	0.514 \pm 0.004	0.685 \pm 0.014	0.857 \pm 0.008	0.986 \pm 0.015	1.055 \pm 0.007	1.142 \pm 0.020	1.192 \pm 0.034
GCN	0.595 \pm 0.006	0.857 \pm 0.018	0.993 \pm 0.012	1.054 \pm 0.034	1.094 \pm 0.043	1.129 \pm 0.061	1.139 \pm 0.075
GAT	0.534 \pm 0.006	0.778 \pm 0.021	0.919 \pm 0.030	1.003 \pm 0.056	1.047 \pm 0.073	1.076 \pm 0.082	1.093 \pm 0.091
ChebNet	0.468 \pm 0.002	0.699 \pm 0.005	0.881 \pm 0.038	1.025 \pm 0.095	1.083 \pm 0.111	1.165 \pm 0.185	1.200 \pm 0.220
Graph Transformer	0.515 \pm 0.001	0.752 \pm 0.005	0.930 \pm 0.013	1.067 \pm 0.036	1.124 \pm 0.033	1.194 \pm 0.080	1.224 \pm 0.104
GraphGPS	0.523 \pm 0.003	0.771 \pm 0.026	0.958 \pm 0.068	1.087 \pm 0.142	1.116 \pm 0.195	1.154 \pm 0.202	1.165 \pm 0.196
EGNN	0.691 \pm 0.006	0.815 \pm 0.004	0.975 \pm 0.026	1.138 \pm 0.078	1.228 \pm 0.079	1.350 \pm 0.173	1.395 \pm 0.187
SchNet	0.685 \pm 0.006	0.844 \pm 0.006	0.949 \pm 0.022	1.068 \pm 0.035	1.157 \pm 0.069	1.270 \pm 0.049	1.342 \pm 0.117
FastEGNN	0.753 \pm 0.015	0.857 \pm 0.001	0.912 \pm 0.007	0.939 \pm 0.011	0.940 \pm 0.010	0.952 \pm 0.008	0.957 \pm 0.001

Table 17: Performance (MCRMSE) of various models in **generalization** experiments on the **Fungal** dataset (mean \pm standard deviation).

Model	0.00	0.05	0.10	0.15	0.20	0.25	0.30
Transformer1D	1.417 \pm 0.005	1.575 \pm 0.002					
GCN	1.192 \pm 0.077	1.230 \pm 0.061	1.256 \pm 0.050	1.280 \pm 0.052	1.290 \pm 0.044	1.328 \pm 0.032	1.333 \pm 0.046
GAT	1.112 \pm 0.035	1.262 \pm 0.115	1.284 \pm 0.102	1.312 \pm 0.092	1.334 \pm 0.087	1.364 \pm 0.080	1.373 \pm 0.072
ChebNet	0.973 \pm 0.003	1.118 \pm 0.008	1.257 \pm 0.018	1.382 \pm 0.022	1.525 \pm 0.020	1.686 \pm 0.030	1.777 \pm 0.033
Graph Transformer	1.317 \pm 0.002	1.407 \pm 0.053	1.418 \pm 0.046	1.427 \pm 0.040	1.439 \pm 0.033	1.447 \pm 0.029	1.456 \pm 0.028
GraphGPS	1.025 \pm 0.081	1.083 \pm 0.011	1.160 \pm 0.006	1.217 \pm 0.012	1.316 \pm 0.026	1.405 \pm 0.040	1.463 \pm 0.052

Table 18: Performance (MCRMSE) of various models in **generalization** experiments on the **Tc-riboswitches** dataset (mean \pm standard deviation).

Model	0.00	0.05	0.10	0.15	0.20	0.25	0.30
Transformer1D	0.705 \pm 0.079	0.711 \pm 0.038	0.732 \pm 0.007	0.753 \pm 0.019	0.815 \pm 0.091	0.803 \pm 0.062	0.796 \pm 0.079
Transformer1D2D	0.633 \pm 0.001	0.705 \pm 0.007	0.745 \pm 0.008	0.749 \pm 0.017	0.800 \pm 0.034	0.766 \pm 0.017	0.754 \pm 0.014
GCN	0.701 \pm 0.004	0.774 \pm 0.026	0.781 \pm 0.051	0.782 \pm 0.062	0.825 \pm 0.093	0.845 \pm 0.072	0.858 \pm 0.126
GAT	0.685 \pm 0.024	0.829 \pm 0.074	0.958 \pm 0.131	0.926 \pm 0.152	1.037 \pm 0.297	0.998 \pm 0.213	1.036 \pm 0.392
ChebNet	0.621 \pm 0.022	0.824 \pm 0.185	0.862 \pm 0.251	0.888 \pm 0.302	0.997 \pm 0.439	0.983 \pm 0.412	1.045 \pm 0.514
Graph Transformer	0.710 \pm 0.041	0.759 \pm 0.035	0.770 \pm 0.047	0.776 \pm 0.054	0.815 \pm 0.101	0.795 \pm 0.085	0.822 \pm 0.115
GraphGPS	0.715 \pm 0.012	0.751 \pm 0.016	0.801 \pm 0.023	0.795 \pm 0.014	0.833 \pm 0.025	0.814 \pm 0.022	0.830 \pm 0.018
EGNN	0.663 \pm 0.010	0.760 \pm 0.043	0.898 \pm 0.134	0.901 \pm 0.123	0.849 \pm 0.053	1.058 \pm 0.239	1.192 \pm 0.453
SchNet	0.655 \pm 0.038	1.368 \pm 0.449	1.099 \pm 0.320	1.419 \pm 0.491	0.900 \pm 0.119	1.957 \pm 0.858	2.025 \pm 0.779
FastEGNN Pooling	0.710 \pm 0.011	0.854 \pm 0.079	0.806 \pm 0.032	0.863 \pm 0.020	0.846 \pm 0.110	0.849 \pm 0.079	0.988 \pm 0.131